systems

MDPI

Article

Inspection-Oriented Predictive Quality Modeling for MDF Manufacturing Using Industrial Process Data and Machine Learning

Roberto Aedo-García [1,*,†], Miguel A. C. Valdebenito-Chavez [2], Silvia E. Restrepo-Medina [3,4], Gerson Rojas Espinoza [5], Javier Zarate Bertoglio [6] and Francisco Ramis-Lanyon [2,*,†]

[1] Departamento de Física, Facultad de Ciencias, Universidad del Bío-Bío, Av. Collao 1202, Concepción 4051381, Chile
[2] Departamento de Ingeniería Industrial, Facultad de Ingeniería, Universidad del Bío-Bío, Av. Collao 1202, Concepción 4051381, Chile
[3] Departamento de Ingeniería Eléctrica, Universidad Católica de la Santísima Concepción, Alonso de Ribera 2850, Concepción 4090541, Chile; srestrepo@ucsc.cl
[4] Centro de Energía, Universidad Católica de la Santísima Concepción, Alonso de Ribera 2850, Concepción 4090541, Chile
[5] Departameto de Ingeniería de Procesos y Bioproductos, Facultad de Ingeniería, Universidad del Bío-Bío, Av. Collao 1202, Concepción 4051381, Chile; grojas@ubiobio.cl
[6] Departamento de TI, Empresa Packing Bio Bio, Av. Oriental N° 6161, Peñalolén 7910000, Chile; gerenteti@pbb.cl
* Correspondence: raedogar@ubiobio.cl (R.A.-G.); framis@ubiobio.cl (F.R.-L.)
† These authors contributed equally to this work.

Highlights

Please indicate how your work links to systems science via your contributions to systems practice, theory, and/or methodology.

- The study conceptualizes continuous MDF manufacturing as a coupled multi-stage system in which disturbances propagate across drying, resin application, forming, and pressing before affecting final product quality.
- It introduces a transferable systems methodology that integrates industrial sensing, target-specific data processing, automated machine learning, and inspection planning within a unified quality-assurance framework.

What are the main findings and/or the implications of the main findings?

- The Vertical Density Profile index (VSC) was predicted consistently for both product families, with test RMSE values of 1.39 and 1.78 index units, whereas Internal Bond prediction depended strongly on product configuration and sensor observability.
- The models can prioritize production intervals for targeted destructive testing, supporting earlier detection of quality drift and faster corrective action without replacing formal laboratory verification.

Check for updates

Academic Editor: Jianhua Zhu

Received: 1 July 2026
Revised: 31 July 2026
Accepted: 6 August 2026
Published: 11 August 2026

Abstract

Continuous medium-density fiberboard (MDF) production presents a persistent quality-assurance problem: destructive laboratory tests return results too late to prevent off-specification material from accumulating before a corrective response is possible. This study develops an inspection-oriented predictive quality framework using industrial Distributed Control System (DCS) data and automated machine learning, treating the production line as an integrated nine-stage system in which upstream process disturbances propagate through coupled thermomechanical and chemical operations before becoming visible in final panel properties. Two quality targets were modeled across Ultralight (UL) and Standard Thin (STD) panels using 3365 production batches and 327 DCS process variables. The pipeline combined Random Forest imputation, Pearson collinearity filtering ($|r| \geq 0.8$), target-specific feature selection, and stacked ensemble regression via H2O AutoML. The Vertical Density Profile Index (VSC), a plant-reported scalar derived from X-ray density profiling, was predicted accurately in both product families (test RMSE: 1.39 and 1.78, index units for UL and STD respectively), reflecting its close coupling to drying stability, resin dosing, and thermal conditions. Internal Bond strength (IB) was harder to predict, especially for thin STD panels (test RMSE: 78.93 kPa vs. 27.41 kPa for UL), as core-layer bonding mechanisms are only indirectly observable through standard DCS instrumentation. Model-agnostic feature importance rankings were physically coherent across both product families, with dominant predictors concentrated in drying, resin application, forming, and hot pressing, consistent with the coupled-subsystem nature of MDF quality formation. The historical dataset was dominated by acceptable and over-quality IB production, which precluded conformity classification and sampling-reduction analysis; a prospective dataset with near-threshold observations is required for those evaluations. Within that scope, the framework provides continuous quality estimates, identifies deviations from the desired operating range, and supports inspection planning as a complement to formal laboratory testing.

Keywords: medium-density fiberboard (MDF); predictive quality control; automated machine learning (AutoML); stacked ensemble; distributed control system (DCS); inspection-oriented decision support; wood-based panels; Industry 4.0

1. Introduction

The medium-density fiberboard (MDF) industry has changed substantially over recent decades due to increasing requirements for product performance, resource efficiency, and raw-material diversification. Production systems that were originally designed for relatively uniform softwood fibers bonded with urea–formaldehyde resin now process a broader range of furnish types, including fast-growing hardwoods, recycled fibers, production residues, and other lignocellulosic materials. These changes support circular-economy and sustainability objectives, but they also increase variability in fiber geometry, chemical composition, bulk density, and moisture content [1–3].

Furnish variability affects fiber formation, adhesive distribution, drying behavior, and heat and mass transfer during hot pressing. Differences in fiber surface chemistry, fines content, moisture, and compressibility modify resin-curing kinetics and the development of the vertical density profile. These effects are subsequently reflected in critical product attributes such as internal bond strength (IB), bending performance, dimensional stability, and thickness swelling [4–6]. The incorporation of recycled raw materials, functional additives, and phase-change materials may further increase the number of interactions that must be controlled during production [1,6].

Continuous MDF manufacturing is therefore better represented as a coupled multi-stage system than as a collection of independent unit operations. Material passes sequentially through fiber preparation, chemical application, drying, forming, pre-pressing, hot pressing, cooling, and finishing operations. Disturbances introduced in an upstream stage may persist, interact with subsequent operating conditions, or become detectable only after the final board has been produced. Final quality consequently emerges from the complete material trajectory through the production line rather than from a single process variable or isolated machine setting [7,8].

https://doi.org/10.3390/systems14080972

From this perspective, MDF quality can be formulated as a latent and partially observed product state. Properties such as IB are not measured continuously during pressing and are known directly only after destructive laboratory testing. During production, the available information consists of indirect and distributed measurements of the conditions under which the material is transformed. These measurements include temperatures, pressures, moisture-related variables, flow rates, resin-dosing signals, equipment loads, and line-speed records. The quality state is only partially observed because some mechanisms that directly influence panel performance, including core temperature, local resin distribution, mat-moisture gradients, and vertical density development, may not be measured online.

Industry 4.0 technologies provide the infrastructure required to analyze this distributed process information. Distributed Control Systems (DCS), Supervisory Control and Data Acquisition systems, and programmable logic controllers continuously record high-dimensional process histories that can be associated with laboratory measurements and production records [8,9]. Within this context, Predictive Quality (PQ) refers to the estimation of product-quality characteristics from manufacturing data before or without an immediate direct measurement of the final property [10]. The resulting estimates can support process monitoring, quality-risk assessment, and decisions concerning when additional inspection is required.

Machine-learning methods are suitable for PQ applications because they can represent nonlinear relationships and interactions among a large number of process variables [9,11,12]. However, predictive performance alone is insufficient for industrial quality assurance. A model may obtain a low average regression error while failing to identify observations close to a product specification limit. Similarly, a model evaluated using randomly partitioned data may produce optimistic results when temporally adjacent production records share raw materials, operating recipes, environmental conditions, and slowly varying equipment states. For industrial deployment, predictive quality models should therefore be evaluated in relation to time, product specifications, model interpretability, and the operational cost of incorrect inspection decisions [10,13].

In MDF production, IB is a particularly important and difficult quality attribute. IB represents tensile resistance perpendicular to the board faces and is influenced by inter-fiber contact, resin distribution, core-layer curing, moisture transport, pressing conditions, and the vertical density profile. Its standard assessment requires destructive testing of specimens taken from completed panels. The resulting measurement is discrete and delayed relative to the continuous production process, limiting the speed with which quality deviations can be identified and corrected. Vertical Density Profile Index (VSC), the second quality response considered in this study, provides complementary information related to material and thermal-process conditions. The two responses therefore represent different levels of observability from routinely recorded process data.

Previous studies have demonstrated that properties of MDF and other wood-based panels can be predicted from laboratory or industrial process variables. André et al. [14] used real plant data, multivariate calibration methods, and genetic-algorithm-based variable selection to predict MDF internal bond strength. Subsequent work developed real-time process models for particleboard properties using variable-selection and regression-ensemble methods [15]. Schubert et al. [16] combined machine and process-control variables with laboratory measurements to predict mechanical properties of industrial wood-fiber insulation boards using Random Forest, artificial neural networks, and support vector machines. Other studies have used artificial neural networks to estimate physical or mechanical properties of MDF and related wood composites [17,18].

More recently, Phetkaew et al. [19] proposed an adaptive controller framework for particleboard manufacturing that combines relevance analysis, pass/fail classification, and decision-tree rules for process adjustment. This study is particularly relevant because it moves beyond continuous-property regression and relates process variables to conformity-oriented decisions. In manufacturing more generally, predictive model-based quality-inspection architectures have integrated data acquisition, preprocessing, model development, and industrial deployment [13]. Automated machine learning has also been investigated as a mechanism for reducing the manual effort required to compare preprocessing strategies, algorithms, and hyperparameters in predictive-quality applications [20]. Consequently, applying H2O AutoML to MDF data is not, by itself, the methodological novelty of the present study.

Table 1 summarizes the principal differences between representative studies and the proposed framework. The comparison shows that previous research has addressed several individual components, including prediction from industrial data, variable selection, nonlinear modeling, pass/fail classification, and predictive-inspection architectures. However, the reviewed literature does not jointly document, for continuous MDF manufacturing, material-oriented temporal alignment across multiple coupled process areas, product-family- and target-specific modeling, chronologically ordered validation, interpretation of the selected final model, evaluation near product-acceptance limits, and simulation of inspection-oriented sampling decisions.

The main research gap is not the lack of machine-learning applications in wood-product manufacturing, but the absence of an integrated framework that connects process-to-product traceability, temporally valid prediction, physically interpretable process information, and evaluation against industrial acceptance criteria in continuous MDF production. A model intended to support inspection must therefore do more than estimate a continuous quality response. It must also identify production intervals that require additional laboratory attention while controlling the risk of missing non-conforming material. To address this gap, this study develops an inspection-oriented predictive-quality framework using industrial DCS and laboratory data. The production line is represented as nine coupled subsystems, and separate models are developed for the Ultralight and Standard Thin product families and for the IB and VSC quality responses. The analysis examines the predictive capacity of routinely recorded multistage variables under chronological validation, the stability and physical consistency of the most relevant process predictors, and the ability of the models to detect production near or outside acceptance limits. H2O AutoML is used as a controlled model-search environment within this workflow and is not considered the primary scientific contribution. The contribution of the study is threefold. Conceptually, MDF quality is represented as a latent and partially observed product state that develops along the material trajectory through coupled thermal, mechanical, and chemical operations. Methodologically, the framework integrates temporal association between process signals and laboratory samples, product- and target-specific modeling, chronological validation, interpretation of the selected final model, and threshold-based evaluation. Operationally, continuous quality predictions are converted into a rule for prioritizing destructive tests and are assessed through sensitivity, false-negative rate, potential sampling reduction, and relative inspection cost. The framework is intended to complement process supervision and formal quality assurance, rather than replace mandatory conformity testing. The central premise is that routinely acquired process variables contain sufficient information to estimate selected MDF quality properties before laboratory results become available. These estimates can support earlier identification of quality drift and more targeted process adjustment when interpreted together with engineering knowledge. The remainder of this paper is organized as follows. Section 2 describes the production system, data sources, temporal alignment, preprocessing, modeling, and validation procedures. Section 3 presents the predictive, inspection-oriented, and model-interpretation results. Section 4 discusses their physical and operational implications, and Section 5 summarizes the main findings, limitations, and future research directions.

Table 1. Comparison of representative predictive-quality studies relevant to wood-panel manufacturing and industrial quality inspection.

Study	Sector or Product	Industrial Data	Process-Stage Coverage	Temporal Alignment	Temporal Validation	Regression Metrics	Inspection Metrics	Sampling or Cost Evaluation
André et al. [14]	MDF	Yes	Multiple process variables; number of physical stages not reported	Not explicitly reported	Not explicitly reported	Yes	No	No
André and Young [15]	Particleboard	Yes	Industrial process variables; number of physical stages not reported	Association by manufacturing time; residence-time correction not reported	Not explicitly reported	Yes	No	No
Schubert et al. [16]	Wood-fiber insulation boards	Yes	Machine and process variables from industrial production	Matched by product type and manufacturing time	No explicit chronological holdout reported	Yes	No	No
Phetkaew et al. [19]	Particleboard	Yes	Process parameters analyzed within a four-step adaptive-control framework	Association through production sampling rounds; residence-time correction not reported	Not explicitly reported	Limited	Yes	No
Krauß et al. [20]	General manufacturing	Yes	Application-dependent predictive-quality datasets	Application dependent	Application dependent	Yes	Application dependent	No explicit sampling-cost simulation
Schmitt et al. [13]	General manufacturing	Yes	Integrated data acquisition, preprocessing, modeling, and deployment architecture	Application dependent	Not explicitly reported	Application dependent	Yes	No wood-panel-specific sampling simulation
Present study	Continuous MDF	Yes	Nine coupled production subsystems	Material-oriented alignment using process lags and aggregation windows	Chronological holdout and blocked validation	Yes	Yes	Sampling reduction and relative-cost simulation

Notes: “Not explicitly reported” indicates that the corresponding methodological element could not be verified in the reviewed publication. “Application dependent” indicates that the study proposed a general framework whose implementation varied across industrial use cases. Regression metrics include measures such as RMSE, MAE, MAPE, or R^2. Inspection metrics include sensitivity, specificity, precision, and false-negative rate.

2. Materials and Methods

This study develops and evaluates predictive models for key quality attributes in continuous MDF manufacturing using industrial process data. The methodological framework integrates plant-level data acquisition, preprocessing, target-specific feature selection, temporal consistency criteria, and supervised machine learning. The MDF production line is treated as a continuous, multi-stage manufacturing system in which upstream disturbances propagate through interconnected thermomechanical and chemical operations before becoming visible in final panel properties. Traceability between process signals, material transformation, and inspection-oriented quality outcomes is maintained at each methodological step.

2.1. Industrial MDF Manufacturing Process Description

Industrial MDF production is a continuous sequence of thermomechanical, chemical, and forming operations that transform raw logs into consolidated panels. The production line analyzed here comprises nine operational stages (A1–A9), shown in Figure 1, which map directly to the plant's Distributed Control System (DCS) architecture. This structure provides traceability between process zones and historical sensor records.

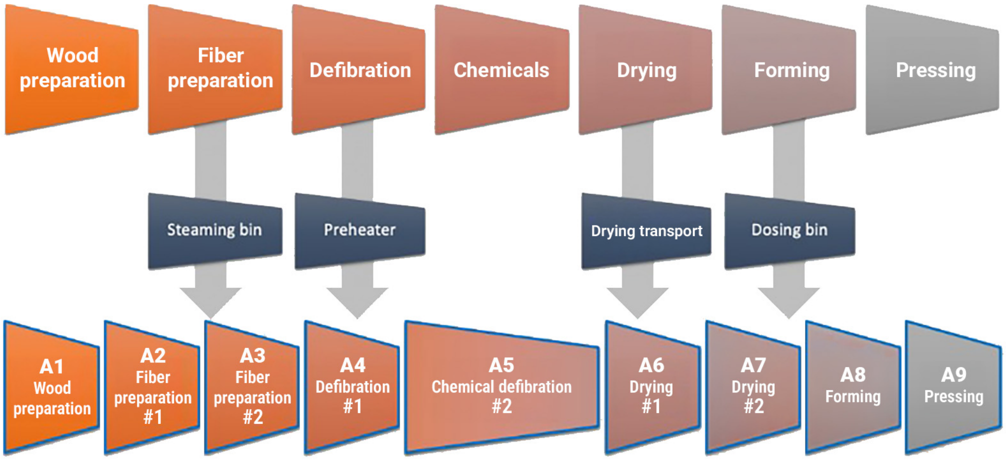

Figure 1. Schematic flow diagram of the medium-density fiberboard (MDF) manufacturing process (A1–A9) analyzed in this study.

The complete process historian contains 327 TAGs distributed across the nine stages, used for online monitoring, process stabilization, and defect prevention. For this study, the MDF line was defined as the manufacturing system bounded by raw material preparation at the inlet and panel release after pressing at the outlet. Main system inputs are raw wood material, steam, thermal energy, and resin-additive formulations; primary outputs are finished MDF panels and their associated quality measurements. Process TAGs serve as observable-state descriptors of the system, while laboratory quality variables provide delayed-response measurements for supervised model development. A complete dictionary of the process tags, including the original plant identifier, a descriptive label, and the coded variable name used during modeling, is provided in Appendix A.

The nine operational stages are summarized below:

- **A1. Wood Preparation:** Raw logs are received, sorted, and conditioned to provide stable feedstock for downstream processing. This stage is monitored by 17 variables and is relevant to limiting variability that may later affect fiber geometry, furnish consistency, and density formation.
- **A2–A3. Fiber Preparation #1 and #2:** Chips undergo size reduction in A2 (21 variables) and thermal conditioning in A3 (10 variables), typically under saturated steam, to improve refining efficiency and fiber softening.

- **A4. Defibration:** Steam-conditioned chips are mechanically refined into fibers. This stage is monitored by 16 variables associated with refining intensity and stock consistency, both of which are relevant for downstream mat formation and bonding behavior.
- **A5. Chemical Defibration #2:** Fibers are blended with urea–formaldehyde (UF) resin and additives. This stage, monitored by 70 variables, regulates dosing, mixing conditions, and temperature, thereby playing a central role in bond formation and panel integrity.
- **A6–A7. Drying #1 and #2:** Moisture is reduced in two consecutive stages to values suitable for the formation and hot pressing. A total of 57 variables describe airflow, temperature, and related operating conditions that affect drying stability and final moisture distribution.
- **A8. Forming:** Resin-treated fibers are distributed to form a mat with controlled basis weight. This stage is monitored by 22 variables related to feeding stability and cross-machine uniformity, which influence the subsequent density profile.
- **A9. Pressing:** The mat is consolidated in a continuous hot press, where densification and resin curing take place. This stage is described by 114 variables, including platen position, thermal conditions, and compression dynamics, and is directly linked to thickness control, curing effectiveness, and delamination risk.

After pressing, panels are discharged for grading and storage. Because final product properties emerge from interactions across all stages, the MDF line is analyzed as an interconnected production system rather than a set of independent unit operations.

2.2. Panel Classes and Process Context

The study covers two commercial MDF product families manufactured on the same continuous line: Ultralight (UL) and Standard Thin (STD). UL panels are produced at densities below 600 kg·m^{-3}, reducing mass while meeting mechanical requirements for non-structural interior applications such as cabinet backings and door skins [3,6]. STD panels correspond to conventional MDF densities, typically within 650 to 750 kg·m^{-3}, but are produced at reduced thicknesses in the range of 2 to 6 mm, prioritizing dimensional precision, surface quality, and machinability for lamination-oriented products (cf. [21]).

Both families pass through the same unit operations: defibration, drying, resin blending, mat forming, and continuous hot pressing. Their density-thickness combinations and target operating windows differ, however, which affects how process variability translates into final board properties. This contrast makes the two families useful for evaluating whether similar process signals retain predictive value across distinct manufacturing regimes.

2.3. Laboratory Quality Measurements

Two laboratory-measured quality responses were analyzed: Internal Bond strength (IB) and the Vertical Density Profile Index (VSC). Both responses were obtained from routine production-quality records associated with the corresponding MDF production intervals. The laboratory results, rather than model predictions, remained the reference measurements for product conformity assessment.

2.3.1. Internal Bond Strength Measurement

Internal Bond strength quantifies the tensile resistance of the panel perpendicular to its faces and serves as an indicator of core-layer bonding and resin-curing effectiveness. The test was conducted according to EN 319 or ASTM D1037 [22,23] using specimens cut from the corresponding panel sampling location. Loading blocks were bonded to both faces, and the specimens were loaded perpendicular to the panel surfaces until failure. Internal Bond strength was calculated as:

$$IB = \frac{F_{\max}}{A}, \quad (1)$$

where $F_{\max}$ is the maximum tensile force recorded at failure (N) and A is the loaded cross-sectional area (mm^2). Results were converted to kPa for modeling and reporting.

The applicable lower acceptance limits were 470 kPa for Ultralight panels and 700 kPa for Standard Thin panels. Values below the corresponding limit were classified as non-conforming.

2.3.2. Vertical Density Profile Index Measurement

In this study, VSC is the identifier used in the plant quality system for the index associated with the vertical density profile of the MDF panel. It does not represent Volatile Solids Content, moisture loss, resin volatility, or any other gravimetric or chemical measurement. The underlying measured property is the variation in local panel density through the complete panel thickness.

The vertical density profile was determined off-line using a laboratory X-ray density profiler manufactured by GreCon (Fagus-GreCon Greten GmbH & Co. KG, Alfeld, Germany). A representative specimen containing the complete panel thickness was extracted from the MDF panel submitted for routine quality control. The specimen was positioned so that the X-ray system scanned sequentially from one panel face to the opposite face. Consequently, the measurement direction was perpendicular to the panel plane and coincident with the thickness direction.

Let h_i denote the measured thickness of specimen i, and let $z \in [0, h_i]$ denote the position through its thickness. During the scan, the instrument recorded the transmitted X-ray intensity at a sequence of positions z_j. The attenuation signal was expressed conceptually as

$$A_i(z_j) = \ln\left(\frac{I_{0,r}}{I_i(z_j)}\right), \quad (2)$$

where $I_{0,r}$ is the reference X-ray intensity for the active instrument calibration or product recipe r, and $I_i(z_j)$ is the intensity transmitted through the specimen at position z_j. The GreCon calibration routine converted attenuation into local density according to

$$\rho_i(z_j) = \mathcal{C}_r\left[A_i(z_j)\right], \quad (3)$$

where $\rho_i(z_j)$ is the local density, expressed in $\mathrm{kg\,m^{-3}}$, and $\mathcal{C}_r$ denotes the equipment calibration function applicable to the panel type, nominal thickness, and measurement configuration.

The complete vertical density profile for specimen i was therefore represented as

$$\mathrm{VDP}_i = \left\{\left(z_j, \rho_i(z_j)\right)\right\}_{j=1}^{N_i}, \quad (4)$$

where N_i is the number of measurement positions generated during the scan. The GreCon software displayed and stored this result as a curve of local density versus position through the panel thickness. This curve captures the high-density surface regions, the transition zones, and the lower-density core region that develop during hot pressing.

For the predictive analyses, the response denoted as VSC was the scalar profile index recorded in the plant quality database and linked to the corresponding GreCon density-profile measurement. The index can be represented as

$$\mathrm{VSC}_i = \mathcal{G}_r(\mathrm{VDP}_i), \quad (5)$$

where $\mathcal{G}_r$ is the profile-processing routine configured in the plant quality-control system for product recipe r. The value exported by this routine was used directly as the response variable. No additional normalization, mass-loss calculation, thermal treatment, or chemical transformation was applied during preparation of the modeling dataset.

The raw density profile and the reported VSC index represent different levels of the same measurement. The raw profile has physical units of kg m^{-3} and retains the spatial distribution of density through the panel thickness. VSC is a unitless plant index that summarizes the measured profile for routine monitoring and historical comparison. It must therefore be interpreted relative to the applicable panel family and product recipe rather than as an absolute density or a material concentration.

The profile is industrially relevant because its shape reflects mat consolidation, heat and moisture transfer, press closing behavior, and density development during hot pressing. High-density surface layers generally contribute to bending stiffness and strength, whereas the density and integrity of the core region are particularly relevant to internal bond strength. Accordingly, VSC was used as an indicator of through-thickness density development and not as a substitute for a specific mechanical test.

VSC was modeled as a continuous response. No universal external pass/fail limit exists for this plant-specific index. For the error-stratified analyses, observations were separated into low, central, and high VSC bands using the first and third quartiles calculated independently for each product family:

$$B_i = \begin{cases} \text{low VSC}, & \text{VSC}_i < Q_{0.25,p}, \\ \text{central VSC}, & Q_{0.25,p} \leq \text{VSC}_i \leq Q_{0.75,p}, \\ \text{high VSC}, & \text{VSC}_i > Q_{0.75,p}, \end{cases} \tag{6}$$

where p identifies the panel family and $Q_{0.25,p}$ and $Q_{0.75,p}$ are the corresponding empirical quartiles. These bands were used solely to examine whether prediction errors changed across the observed VSC range. They were not treated as regulatory conformity limits or as replacements for the plant's controlled product specifications.

Table 2 summarizes the measurement basis, reported scale, and industrial interpretation of the two quality responses used in the predictive analysis.

Table 2. Definition and industrial interpretation of the quality responses used in the predictive models.

Response	Measured Property	Laboratory Procedure	Reported Scale	Analysis Rule	Practical Interpretation
IB	Tensile strength perpendicular to the panel faces	A specimen extracted from the finished MDF panel was bonded to loading blocks and subjected to tensile loading perpendicular to the panel plane until failure.	kPa	Continuous response; product conformity is assessed against the applicable product-specific lower limit.	Low values indicate insufficient bonding or curing in the panel core and may be associated with unfavorable core-density development.
VSC	Plant-reported index derived from the vertical density profile of the finished MDF panel	A full-thickness specimen was scanned perpendicular to the panel plane using a GreCon X-ray density profiler. Calibrated X-ray attenuation was converted into local density, producing a density-versus-thickness curve. The scalar VSC value stored in the quality database was used without further transformation.	Unitless plant index; underlying profile in kg m^{-3} versus thickness	Continuous response. Product-specific empirical quartiles were used only to stratify prediction errors into low, central, and high VSC bands.	Describes through-thickness density development, including the surface density peaks, transition regions, and core-density zone formed during hot pressing. It is not a volatile-solids or mass-loss measurement.

For both Ultralight and Standard Thin panels, the VSC index ranged from approximately 80 to 100 across the training subset.

2.4. Data Acquisition and Experimental Context

Historical operational records from an industrial MDF facility were consolidated into a dataset of 3365 production batches and 356 variables, classified into three groups:

- **Temporal variables** (10): timestamp-related variables used for process traceability and exploratory inspection but excluded from predictive training.
- **Quality variables** (19): laboratory-derived product measurements considered as candidate response variables.
- **Process variables** (327): DCS TAGs recorded across the nine production zones (A1–A9), identified using the notation A_{i_j}, where i denotes the process area and j the sensor identifier.

Data auditing revealed extensive missingness in several laboratory quality variables, attributable to selective testing practices, particularly in UL production cycles. Variables including MOE, MOR, Water Absorption, and Thickness Swelling showed missingness rates above 68%. Under a conventional 70/20/10 split, these variables would yield test subsets too small for reliable generalization assessment and were therefore excluded from the modeling scope. Missing values in process predictors were handled by Random Forest (RF)-based multivariate imputation, selected for its ability to preserve nonlinear dependencies among industrial variables without imposing distributional assumptions that are rarely appropriate in MDF process data. Imputation was applied only to predictor variables; quality responses were never imputed, preventing leakage of laboratory information into the feature space.

For UL panels, 47 process variables required imputation. A Pearson collinearity filter with threshold $|r| \geq 0.8$ then removed 129 redundant predictors, leaving a candidate set of 154 variables (Table 3). For STD panels, 42 variables required imputation and 137 collinear predictors were removed, leaving 148 variables (Table 4).

The threshold $|r| \geq 0.8$ was chosen as a conservative criterion that reduces redundancy while retaining complementary information. In industrial environments, highly correlated TAGs typically reflect shared actuators, derived variables, or common control loops. Removing them improves numerical stability and interpretability without eliminating the capacity of ensemble or neural methods to capture nonlinear process interactions.

Table 3. Missing data and collinearity reduction summary for Ultralight (UL) panels.

Preprocessing Step	Affected Variables	Method/Threshold	Outcome
Missing Data	47 variables	Random Forest Imputation	All missing values estimated
Collinearity Filter	129 variables	Pearson $\lvert r \rvert \geq 0.8$	Removed from feature space
Post-filter Variable Set	154 variables	–	Retained for modeling

Variables correspond mainly to process signals from hot pressing, resin application, and drying sections.

Table 4. Missing data and collinearity reduction summary for Standard Thin (STD) panels.

Preprocessing Step	Affected Variables	Method/Threshold	Outcome
Missing Data	42 variables	Random Forest Imputation	All missing values estimated
Collinearity Filter	137 variables	Pearson $\lvert r \rvert \geq 0.8$	Removed from feature space
Post-filter Variable Set	148 variables	–	Retained for modeling

Variables correspond mainly to process signals from hot pressing, resin application, and drying sections.

https://doi.org/10.3390/systems14080972

2.5. Exploratory Data Analysis and Variable Selection

Exploratory analysis and feature screening were conducted separately for UL and STD panels to preserve the distinction between product classes and their operating regimes. Although the plant historian stores 327 DCS TAGs, class-specific candidate sets were smaller because some signals were inactive, quasi-constant, or inconsistently recorded during particular campaigns. After this screening, UL models started from 283 candidate predictors and STD models from 285. A comparative summary of the preprocessing and target-specific feature selection results is presented in Table 5.

Table 5. Comparative preprocessing and target-specific feature selection for UL and STD MDF panels.

Feature	Ultralight (UL)	Standard Thin (STD)
Initial candidate predictors	283	285
Post-collinearity predictors	154	148
Collinear variables removed	129	137
Predictors imputed (RF)	47	42
Final IB predictors	55	56
Final VSC predictors	72	75
Top correlated tag (IB)	0.31 (`A9_24`)	`A9_53`
Top correlated tag (VSC)	0.32 (`A6_29`)	–

The preprocessing pipeline was identical for both product families: RF-based imputation, Pearson collinearity filtering, and target-specific feature selection. This shared structure ensures comparability while allowing the final predictor sets to remain specific to each quality target.

For UL panels, 47 predictors required imputation and 129 collinear variables were removed, leaving 154 non-redundant predictors. Target-specific selection produced distinct feature sets for each response. For Internal Bond (IB), 56 predictors passed the correlation screen and 55 were retained after importance-based pruning; the strongest linear association was observed for `A9_24` ($r \approx 0.31$). For Vertical Density Profile Index (VSC), 72 predictors met the screening criterion and were retained, with `A6_29` showing the strongest linear association ($r \approx 0.32$).

For STD panels, 42 predictors were imputed and 137 collinear variables removed, yielding 148 predictors. For IB, 60 predictors passed the correlation screen and 56 remained after importance-based filtering, with `A9_53` among the most relevant contributors. For VSC, 77 predictors were initially selected and 75 retained after pruning. The quality targets depend on partially overlapping but non-identical subsets of process signals. VSC is associated with a broader set of process conditions than IB within the screened variable space. The strongest pairwise correlations remained modest ($|r| \approx 0.31$ to 0.32), consistent with quality outcomes that arise from coupled process interactions rather than any single dominant sensor signal. Correlation screening served exclusively as an initial dimensionality-reduction step, not as evidence of direct causality. Variable retention was interpreted in operational and predictive terms: identifying potentially informative signals prior to multivariate model fitting.

2.6. Temporal Alignment and Material Tracking in Continuous Production

In continuous MDF manufacturing, process variables must be associated with the same material segment that is subsequently evaluated in the laboratory. Measurements generated during wood preparation, refining, chemical application, drying, forming, and pressing occur at different times, although they describe successive transformations of the same product. An incorrect temporal association may therefore link a laboratory result to process conditions belonging to another production interval and reduce the physical validity of the predictive model.

Previous studies have shown that upstream variables such as refining conditions, motor load, and energy consumption can provide early information about downstream product properties [7,24,25]. Variables related to mat consolidation, press geometry, panel thickness, and density development have also been associated with mechanical quality [7,26,27]. Similarly, surface roughness, drilling response, water absorption, and thickness swelling retain information from previous machining, additive-dosing, and pressing conditions [28–30]. These findings support a material-oriented alignment procedure rather than direct matching based only on the laboratory timestamp.

For each laboratory observation, the material trajectory was reconstructed backward from the timestamp recorded by the Human–Machine Interface (HMI) at the continuous press. This reference time was denoted by t_1. The estimated passage times through the upstream process areas, $t_2, \ldots, t_9$, were calculated recursively using known transport distances, nominal residence times, press-belt speed, and dosing-bin level.

The timestamp associated with the forming section was calculated from the distance to the press:

$$t_2 = t_1 - \frac{L_{\text{forming}}}{v_{\text{press},i}} \times 60, \tag{7}$$

where $L_{\text{forming}} = 100$ m and $v_{\text{press},i}$ is the press-belt speed for production record i, expressed in $\text{m}\,\text{min}^{-1}$. The factor 60 converts the calculated travel time to seconds.

The delay associated with the second drying section was adjusted using the recorded dosing-bin level:

$$t_3 = t_2 - 600\left(\frac{B_i}{100}\right), \tag{8}$$

where B_i is the dosing-bin level expressed as a percentage. The division by 100 converts the recorded value to a fraction between 0 and 1.

The remaining upstream timestamps were calculated using fixed transport or residence-time corrections:

$$t_4 = t_3 - 120, \tag{9}$$

$$t_5 = t_4 - 15, \tag{10}$$

$$t_6 = t_5 - (3.3 \times 60), \tag{11}$$

$$t_7 = t_6 - 20, \tag{12}$$

$$t_8 = t_7 - 420, \tag{13}$$

$$t_9 = t_8 - 30. \tag{14}$$

The fixed delays in Equations (9)–(14) were derived from nominal transport distances and residence times documented in the plant engineering records, not from data-driven lag optimization. All delays in Equations (9)–(14) are expressed in seconds. The reconstructed timestamps correspond, respectively, to Drying #1, Refining #2 and chemical addition, Refining #1, Fiber Preparation #2, Fiber Preparation #1, and Wood Preparation.

For process area a, the reconstructed timestamp $t_{i,a}$ was used as the temporal reference for laboratory sample i. The associated aggregation interval was defined as

$$W_{i,a} = \left[t_{i,a} - \Delta_a^-, t_{i,a} + \Delta_a^+\right], \tag{15}$$

where Δ_a^- and Δ_a^+ denote the backward and forward limits of the area-specific window. DCS observations contained within this interval were assigned to the corresponding material segment. For continuously sampled variable j, the representative value was calculated as

$$\overline{x}_{i,j} = \frac{1}{n_{i,a}} \sum_{t \in W_{i,a}} x_j(t), \tag{16}$$

where $x_j(t)$ is the recorded DCS signal and $n_{i,a}$ is the number of valid measurements within the aligned interval. Variables already stored as batch-level statistics in the production database were used without additional temporal averaging.

The alignment procedure was based on engineering residence-time relations rather than data-driven lag optimization. Correlation-based methods, including cross-correlation, distance correlation, and maximal information coefficient, can be useful when physical residence times are unknown [31]. In this study, however, they were not used to replace the known production-sequence relationships. This choice preserves the physical interpretation of the aligned predictors and avoids selecting temporal delays solely according to their association with the target variable.

Production intervals identified as stoppages, start-ups, incomplete production cycles, or product transitions were excluded when a consistent material trajectory could not be established. No temporal interpolation was performed across these intervals. Records with incomplete timestamp sequences or insufficient DCS coverage within the corresponding aggregation window were also removed. Ultralight and Standard Thin observations were subsequently modeled separately to avoid combining distinct operating regimes.

This treatment is relevant because stoppages and transitions may produce valid sensor readings that do not represent stable material flow [24]. The resulting predictor vectors therefore represent physically consistent sequences of operating conditions experienced by the material before laboratory testing.

For long-term deployment, temporal alignment must be complemented by dataset versioning, operating-mode labeling, and monitoring of missing data and process drift. Structured real-time data pipelines facilitate model traceability and iterative updating in cyber-physical and digital-twin environments [32]. Changes in raw materials, recipes, equipment condition, or sensor calibration may produce temporal performance degradation and should be monitored during industrial operation [33,34].

2.7. Data Partition and Distributional Assessment

For each product family and quality response, the available observations were randomly divided into training, validation, and test subsets using proportions of 70%, 20%, and 10%, respectively. The partition was performed independently for each product–target combination. The resulting sample sizes were 1189/329/162 for Ultralight IB, 1195/327/158 for Ultralight VSC, 489/157/69 for Standard Thin IB, and 502/146/67 for Standard Thin VSC in the training, validation, and test subsets, respectively.

To determine whether random allocation produced systematic differences in the marginal distributions of the quality responses, the training, validation, and test subsets were compared using complementary non-parametric procedures. Pairwise two-sample Kolmogorov–Smirnov tests were used to compare the complete empirical distributions, the Kruskal–Wallis test was used to assess differences in central location, and the Brown–Forsythe test was used to evaluate differences in dispersion.

For subsets g and h, the Kolmogorov–Smirnov statistic was defined as

$$D_{g,h} = \sup_{y} \left| F_g(y) - F_h(y) \right|, \tag{17}$$

where $F_g(y)$ and $F_h(y)$ are the corresponding empirical cumulative distribution functions.

Differences in central location were evaluated using the Kruskal–Wallis statistic,

$$H = \frac{12}{N(N+1)} \sum_{g=1}^{G} \frac{R_g^2}{n_g} - 3(N+1), \quad (18)$$

where $G = 3$ represents the training, validation, and test subsets, n_g is the number of observations in subset g, R_g is the sum of ranks in that subset, and $N = \sum_{g=1}^{G} n_g$.

Dispersion was assessed using the Brown–Forsythe transformation,

$$z_{ig} = |y_{ig} - \tilde{y}_g|, \quad (19)$$

where y_{ig} is observation i in subset g, and $\tilde{y}_g$ is the corresponding group median. An analysis of variance was then applied to the transformed values z_{ig}.

For all tests, the null hypothesis stated that the corresponding distributional characteristic did not differ among subsets. A significance level of $\alpha = 0.05$ was adopted. The inferential analysis was complemented by comparisons of the mean, median, standard deviation, interquartile range, and observed range of IB and VSC.

These tests were used to assess distributional balance after random partitioning. They were not interpreted as evidence of temporal independence between adjacent production batches.

2.8. Model Development and Evaluation

Supervised regression models were developed to predict two laboratory-measured quality attributes in industrial MDF manufacturing: Internal Bond strength (IB, kPa) and the Vertical Density Profile Index (VSC, unitless index). In this study, VSC was treated as a plant-reported quality indicator used for industrial process monitoring rather than as a direct compositional measurement.

Separate models were developed for Ultralight and Standard Thin panels using production data collected between June 2017 and June 2018. The predictor set combined process measurements from nine production areas (A1–A9) with the corresponding laboratory quality observations. Because laboratory assays were recorded less frequently than the DCS signals, the modeling task involved estimating sparse quality responses from a high-dimensional process dataset.

For each product family and target variable, the curated observations were divided into training, validation, and test subsets using proportions of 70%, 20%, and 10%, respectively, as described in Section 2.7. The training subset was used to fit candidate models, the validation subset was used for model comparison and selection, and the test subset was reserved for the final hold-out evaluation.

Model development was conducted using the `H2O AutoML` (version 3.42, H2O.ai, Mountain View, CA, USA) framework [35]. The candidate model family included Gradient Boosting Machines (GBM), Distributed Random Forests (DRF), Extremely Randomized Trees (XRT), Deep Neural Networks (DNN), and Generalized Linear Models (GLM). AutoML also generated stacked ensembles by combining selected base learners through a metalearning procedure.

Candidate models were ranked using validation Root Mean Squared Error (RMSE) as the primary selection criterion. Mean Absolute Error (MAE) was used as a complementary metric to assess average prediction deviation. The selected model was determined independently for each product–target combination. A stacked ensemble was retained only when it achieved the lowest validation RMSE; otherwise, the highest-ranked individual learner was selected. Model identity and hyperparameters were fixed before predictions were generated for the test subset.

https://doi.org/10.3390/systems14080972

The test subset was not used for model ranking, hyperparameter adjustment, feature selection, or replacement of the selected model. Its sole purpose was to estimate the hold-out predictive performance of the model selected during the training and validation stages. The complete modeling procedure is summarized in Figure 2.

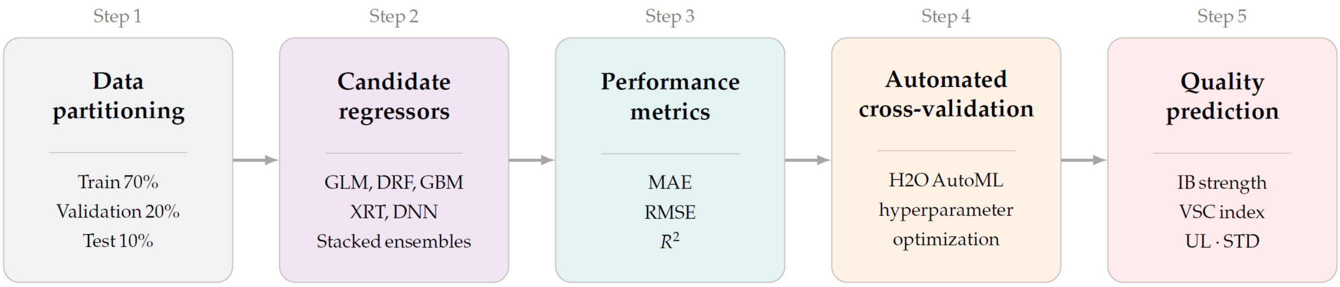

Figure 2. Predictive modeling workflow for MDF quality estimation using `H2O AutoML`. Separate models were developed for IB and VSC in Ultralight and Standard Thin panels. Candidate models were fitted using the training subset, compared using validation RMSE, and evaluated on the held-out test subset after model selection.

Predictive performance on the test subset was quantified using Mean Absolute Error (MAE), Root Mean Squared Error (RMSE), and the coefficient of determination (R^2). MAE and RMSE were calculated as

$$\mathrm{MAE} = \frac{1}{n}\sum_{i=1}^{n}|y_i - \hat{y}_i|, \tag{20}$$

$$\mathrm{RMSE} = \sqrt{\frac{1}{n}\sum_{i=1}^{n}(y_i - \hat{y}_i)^2}, \tag{21}$$

and R^2 was calculated as

$$R^2 = 1 - \frac{\sum_{i=1}^{n}(y_i - \hat{y}_i)^2}{\sum_{i=1}^{n}(y_i - \bar{y})^2}, \tag{22}$$

where y_i and $\hat{y}_i$ are the observed and predicted values, respectively, $\bar{y}$ is the mean of the observed target values in the test subset, and n is the number of test observations.

RMSE was used as the main performance metric because it gives greater weight to large prediction errors, which are relevant in industrial quality-control applications. MAE provided a complementary measure of the typical prediction error, while R^2 described the proportion of response variability represented by the model.

Because the intended application is inspection support, the regression metrics were interpreted as measures of predictive error rather than as direct evidence of conformity-classification performance. The ability of the models to prioritize laboratory testing or identify non-conforming production requires a separate threshold-based evaluation using metrics such as sensitivity, specificity, precision, and false-negative rate.

To interpret the final stacked ensemble, model-agnostic permutation feature importance was calculated directly from the ensemble prediction function. For each response, the independent test set was first evaluated without perturbation. Each predictor was subsequently permuted 30 times while all remaining predictors were held unchanged. Feature importance was quantified as the mean increase in RMSE, and the standard deviation across permutations was retained as an uncertainty measure. Global SHAP values were additionally estimated using a permutation-based model-agnostic explainer with 40 training observations as the background distribution and 50 test observations for global interpretation. SHAP importance was expressed as the mean absolute contribution of each predictor. Ranking stability was evaluated by recalculating permutation importance on the training, validation and test partitions. Pairwise Spearman correlations, Kendall's coefficient of concordance, mean rank, rank standard deviation and top-10 selection frequency were used to quantify stability.

3. Results

The results are presented in six parts. First, the distributional balance of the training, validation, and test subsets is examined. Second, the observed IB distributions are compared with the operating quality ranges for both product families. Third, predictive performance is reported for each product–target combination. Fourth, the error structure is evaluated across the observed quality range. Fifth, the process variables associated with model predictions are examined. Finally, the implications and limitations of the models for inspection support are discussed.

Because the data subsets were obtained through random allocation, the reported test metrics represent hold-out performance under distributionally comparable operating conditions. They should not be interpreted as prospective validation on a later production period.

3.1. Distributional Balance Across Data Subsets

Table 6 presents the statistical comparison of IB and VSC across the training, validation, and test subsets.

Table 6. Distributional comparison of IB and VSC across the training, validation, and test subsets.

Product	Target	Kruskal–Wallis p	Brown–Forsythe p	KS Train–Validation p	KS Train–Test p	KS Validation–Test p	Interpretation
UL	IB	0.3833	0.9614	0.7444	0.4595	0.9074	No significant differences in location, dispersion, or empirical distribution.
UL	VSC	0.6428	**0.0345**	0.3764	0.5765	0.9901	Comparable location and empirical distributions, with a modest difference in dispersion.
STD	IB	0.2923	0.0577	0.4135	0.1698	0.1901	No significant differences in location, dispersion, or empirical distribution.
STD	VSC	0.6071	0.7388	0.9720	0.8088	0.5984	No significant differences in location, dispersion, or empirical distribution.

Notes: UL denotes Ultralight MDF, STD denotes Standard Thin MDF, and KS denotes the two-sample Kolmogorov–Smirnov test. The Kruskal–Wallis test evaluates differences in central location, whereas the Brown–Forsythe test evaluates differences in dispersion around the subset medians. Bold type identifies $p < 0.05$.

For Ultralight IB, none of the tests indicated significant differences among the three subsets. The Kruskal–Wallis test yielded $p = 0.3833$, the Brown–Forsythe test yielded $p = 0.9614$, and all pairwise Kolmogorov–Smirnov comparisons were non-significant. Standard Thin IB showed a similar pattern, with no significant differences in central location, dispersion, or empirical distribution.

For Ultralight VSC, the Kruskal–Wallis and pairwise Kolmogorov–Smirnov tests indicated comparable central values and empirical distributions. The Brown–Forsythe test detected a difference in dispersion ($p = 0.0345$). The magnitude of this difference was limited, with standard deviations of 1.89, 1.98, and 2.08 index units for the training, validation, and test subsets, respectively.

For Standard Thin VSC, none of the tests identified significant differences among the subsets. Overall, the random partition preserved similar marginal distributions of IB and VSC, with the exception of the small increase in dispersion observed for Ultralight VSC.

These findings support the use of the three subsets for model fitting, selection, and hold-out evaluation under broadly comparable response distributions. They do not demonstrate temporal independence and should not be interpreted as chronological or prospective validation.

3.2. IB Distribution Relative to the Operating Quality Range

The IB distributions were examined relative to the operating quality ranges used for the two MDF product families. For Ultralight panels, the reference interval was 520–600 kPa. The training subset had a mean of 626.61 kPa and a median of 625.00 kPa, placing the center of the distribution above the upper reference limit.

As shown in Figure 3, the historical IB data were concentrated mainly above the operating quality ranges. For Ultralight panels, the mean and median exceeded the upper reference limit of 600 kPa. The displacement was more pronounced for Standard Thin panels, whose mean and median were substantially higher than the upper reference limit of 870 kPa.

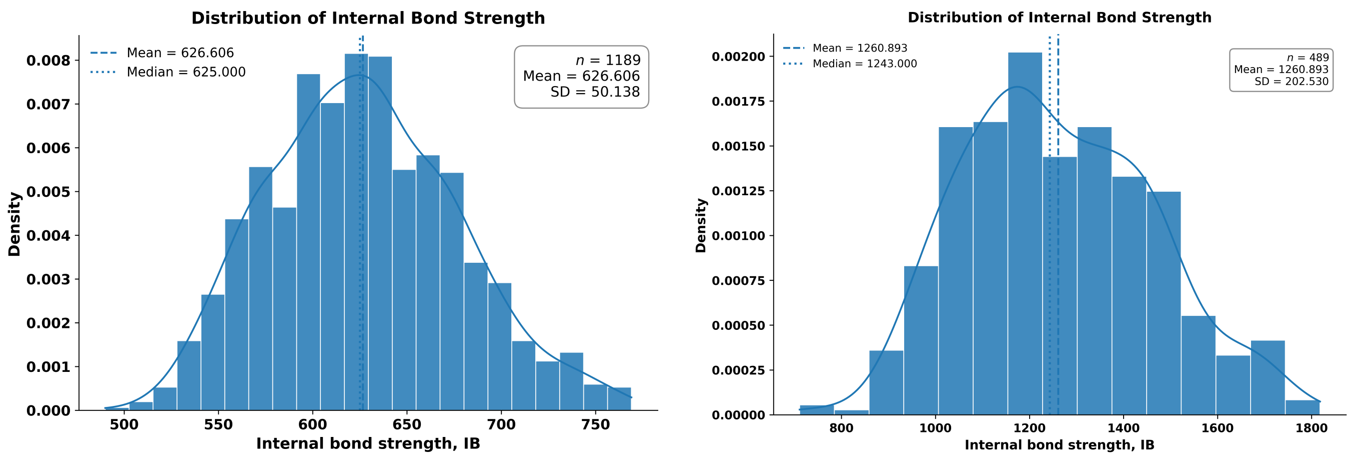

Figure 3. Distribution of Internal Bond strength relative to the operating quality ranges. (**a**) Ultralight MDF training subset ($n = 1189$): the observed mean and median were 626.61 and 625.00 kPa, respectively, compared with an operating reference range of 520–600 kPa. (**b**) Standard Thin MDF training subset ($n = 489$): the observed mean and median were 1260.89 and 1243.00 kPa, respectively, compared with an operating reference range of 750–870 kPa.

The observed pattern indicates that the dataset was dominated by acceptable and over-quality production rather than by recurrent low-IB events. In operational terms, the principal condition represented in the data was therefore systematic quality giveaway.

This result is relevant for process control because IB values above the required range may reflect operating conditions that are more intensive than necessary. Possible contributors include resin application, thermal input, pressing intensity, or interactions among these variables. The observational data do not support direct attribution to a specific process factor, but the distributional shift identifies a potential opportunity for process adjustment while maintaining the applicable quality requirement.

The limited number of observations near or below the lower acceptance limits also restricts a conventional conformity-classification analysis. Sensitivity, specificity, precision, and false-negative rate cannot be estimated robustly when the non-conforming class is poorly represented. For the same reason, a sampling-reduction or inspection-cost simulation would not provide a reliable estimate of the risk of missing non-conforming production.

The models are therefore interpreted in this study as continuous quality estimators and over-quality monitoring tools rather than as validated conformity classifiers. A prospective dataset containing sufficient near-threshold and non-conforming observations would be required to assess conformity detection, destructive-sampling reduction, and inspection-cost trade-offs.

3.3. Predictive Performance on Held-Out Production Data

Model performance was evaluated using the randomly held-out test subset, which was excluded from model fitting, hyperparameter adjustment, and model selection. Predictive performance was quantified using Root Mean Squared Error (RMSE) and Mean Absolute Error (MAE), expressed in the native scale of each response: Internal Bond strength (IB, kPa) and Vertical Density Profile Index (VSC, unitless index).

Model benchmarking was conducted using `H2O AutoML`. Candidate models were fitted using the training subset and ranked independently for each product–target combination according to validation RMSE. MAE was used as a complementary metric. Once the highest-ranked candidate had been identified, its model specification was fixed and the test subset was used only for the final hold-out evaluation [10,35].

3.3.1. Internal Bond Strength Prediction Performance

Table 7 identifies the model selected from the validation results for each product–target combination and reports its subsequent hold-out test performance. For Ultralight panels, the IB model achieved an RMSE of 27.41 kPa and an MAE of 18.71 kPa. For Standard Thin panels, the corresponding values were 78.93 kPa and 49.68 kPa.

Table 7. Selected models and their performance on the validation and held-out test subsets. Models were ranked by validation RMSE independently for each product–target combination; the test subset was evaluated only after model selection was complete.

Panel Type	Target	Selected Model	Val. RMSE	Val. MAE	Test RMSE	Test MAE	Test *n*
Ultralight	IB	Stacked Ensemble—Best of Family (5 base models: 1 GBM, 1 XGBoost, 2 DRF, 1 DNN; metalearner: GLM, 5-fold CV)	41.24	35.59	27.41	18.71	162
Ultralight	VSC	Stacked Ensemble—All Models (8 of 20 base models: 3 GBM, 1 XGBoost, 1 DRF, 3 DNN; metalearner: GLM, 5-fold CV)	1.41	1.08	1.39	1.11	158
Standard Thin	IB	Stacked Ensemble—All Models (8 of 20 base models: 2 GBM, 2 XGBoost, 3 DNN, 1 DRF; metalearner: GLM, 5-fold CV)	150.24	117.74	78.93	49.68	69
Standard Thin	VSC	Stacked Ensemble—Best of Family (4 base models: 1 GBM, 1 XGBoost, 1 DNN, 1 GLM; metalearner: GLM, 5-fold CV)	2.13	1.60	1.78	1.31	67

Notes: Val. = validation subset. RMSE and MAE for IB are expressed in kPa; for VSC, in index units. Stacked Ensemble Best of Family combines the single best model from each algorithm family; Stacked Ensemble All Models draws from the full candidate pool. In both cases the metalearner was a GLM fitted on 5-fold cross-validated predictions from the base models. The number of base models actually used by the metalearner (selected column) may be smaller than the total trained, as the GLM regularization can assign zero weight to some candidates. Test metrics were computed after model selection was fixed and were not used to rank or replace candidates.

The larger errors obtained for Standard Thin panels indicate that the available DCS variables represented IB variation less effectively for this product family. This result is consistent with the sensitivity of thin panels to local variation in mat formation, moisture distribution, and press behavior, although the observational data do not permit a causal attribution of the error difference [7].

Figure 4 compares observed and predicted values for Ultralight panels across the three subsets. Predictions remain generally centered around the 1:1 line, while larger residuals occur mainly near the extremes of the observed range. Because the subsets were randomly sampled from the same production period, differences among them are interpreted as hold-out variation rather than as evidence of performance under future operating conditions.

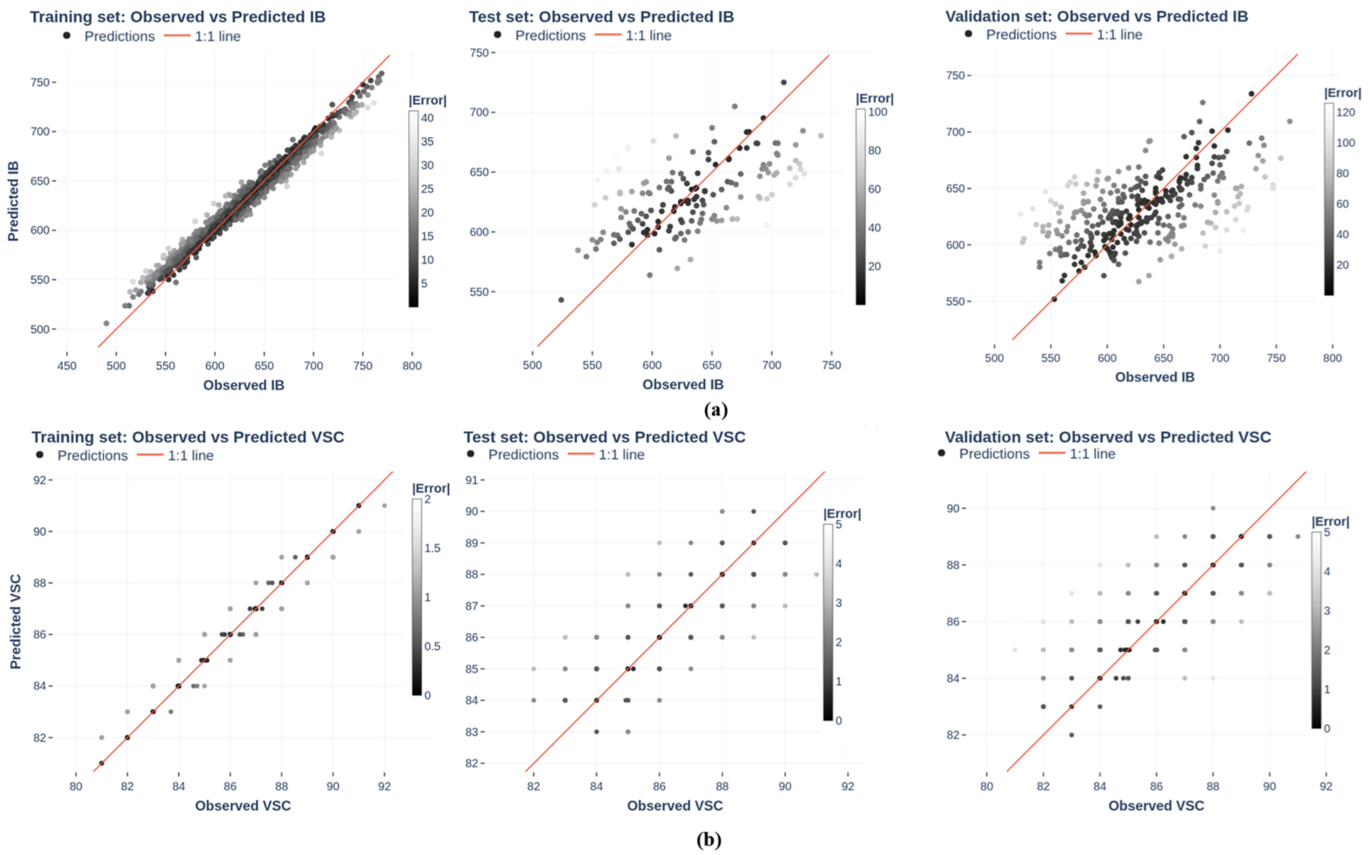

Figure 4. Observed and predicted quality responses for Ultralight MDF. (**a**) Internal Bond strength and (**b**) Vertical Density Profile Index across the training, validation, and test subsets. The diagonal represents perfect agreement.

3.3.2. Vertical Density Profile Index Prediction Performance

For Ultralight panels, the selected VSC model achieved a validation RMSE of 1.41 and a test RMSE of 1.39. The corresponding MAE values were 1.08 and 1.11, respectively. For Standard Thin panels, validation and test RMSE were 2.13 and 1.78, while MAE was 1.60 and 1.31.

Because IB and VSC are reported on different scales, their absolute error values are not directly comparable. The similar validation and test errors observed for VSC indicate stable hold-out performance within the randomly partitioned production data. This result should not be interpreted as evidence of prospective performance on a later production period.

3.3.3. Observed and Predicted Trends Across the Response Range

Figure 5 compares observed and predicted IB values for Ultralight and Standard Thin panels across the three subsets, with samples ordered by observed IB. This representation shows how prediction fidelity changes across the response range.

For Ultralight panels, the predicted curve follows the observed pattern with moderate local deviations. For Standard Thin panels, the mismatch is more pronounced, particularly where the observed response changes abruptly. This pattern is consistent with the larger errors reported in Table 7.

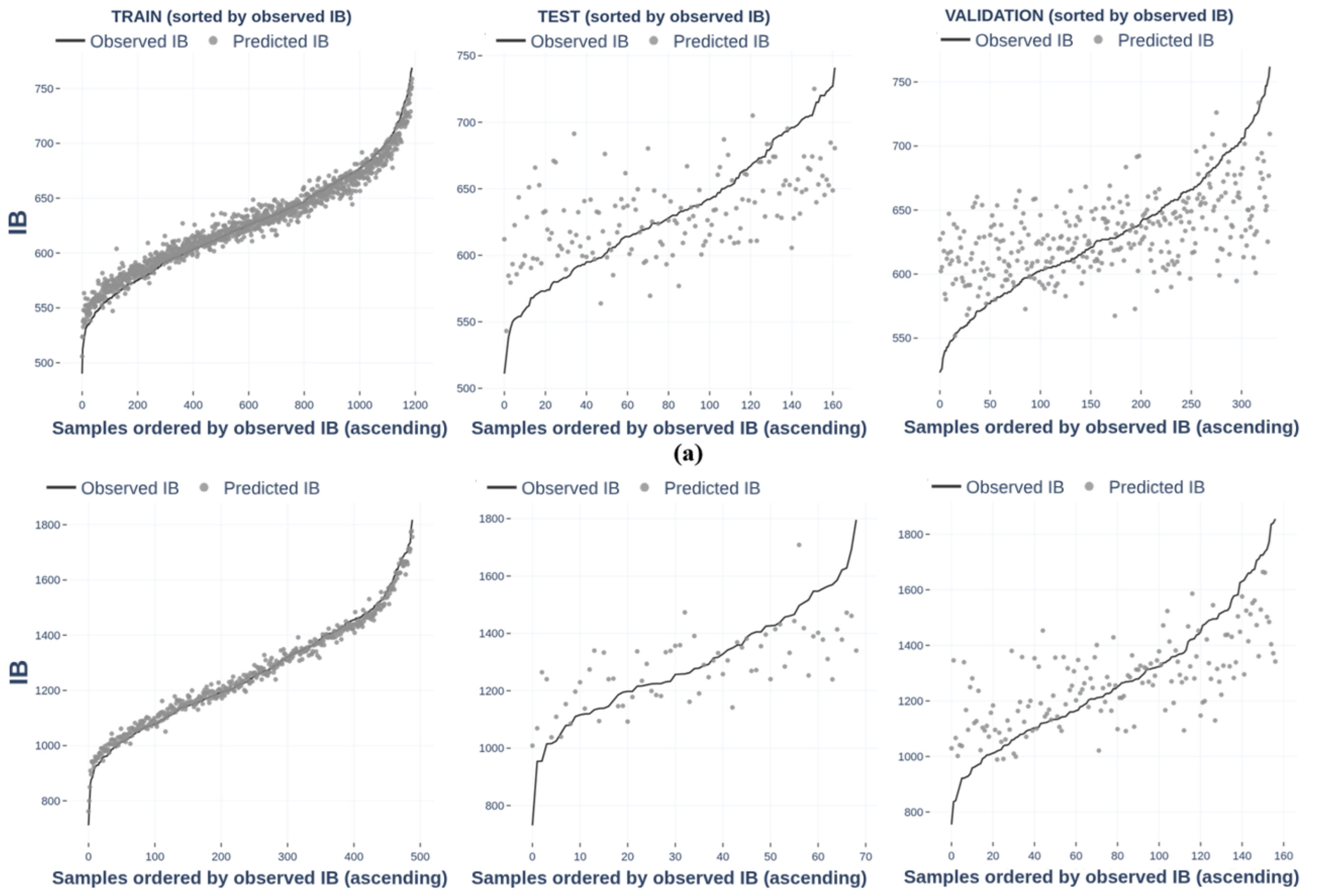

(a) **(b)**

Figure 5. Observed and predicted Internal Bond strength for (**a**) Ultralight and (**b**) Standard Thin MDF across the training, validation, and test subsets. Samples are ordered by observed IB.

3.4. Error Structure and Relevance for Inspection Support

Aggregate regression metrics were complemented by graphical analysis of the error structure across the observed quality range. The parity and response-ordered plots show that prediction errors were distributed across the response range, although larger deviations occurred near some extreme observations.

For Ultralight IB, the mean percentage errors were 3.16%, 2.98%, and 2.82% in the low-, normal-, and high-quality bands, respectively. For Ultralight VSC, the corresponding values were 1.31%, 1.29%, and 1.26%. These results indicate that the average relative error did not concentrate strongly in one quality band.

The percentage-error analysis describes the distribution of continuous prediction errors, but it does not establish conformity-detection performance. As shown in Figure 3, the available IB observations were concentrated mainly above the operating quality ranges, particularly for Standard Thin panels. The number of observations near or below the lower acceptance limits was therefore insufficient for a stable estimation of sensitivity, specificity, precision, and false-negative rate.

For this reason, no inspection-cost or sampling-reduction simulation was introduced. Such a simulation would require reliable estimates of the probability of missing non-conforming production, which cannot be obtained from a dataset dominated by acceptable and over-quality observations. The present models should instead be interpreted as continuous monitoring tools that can identify deviations from the desired operating range, including persistent over-quality.

3.5. Process-Relevant Predictive Drivers

The selected model differed according to the product–target combination. Because the available global importance rankings were obtained from an individual GBM, they were used as an auxiliary analysis of predictive relevance within that learner. These rankings should not be interpreted as a direct explanation of the selected model when the final candidate corresponded to another algorithm or to a stacked ensemble.

Figure 6 presents the global feature-importance rankings for IB prediction in Ultralight and Standard Thin panels. In both cases, the leading tags are concentrated in areas associated with drying, resin and additive application, and hot pressing. These variables were informative within the GBM model and are physically consistent with known mechanisms related to moisture conditioning, dosing stability, and thermal-mechanical consolidation.

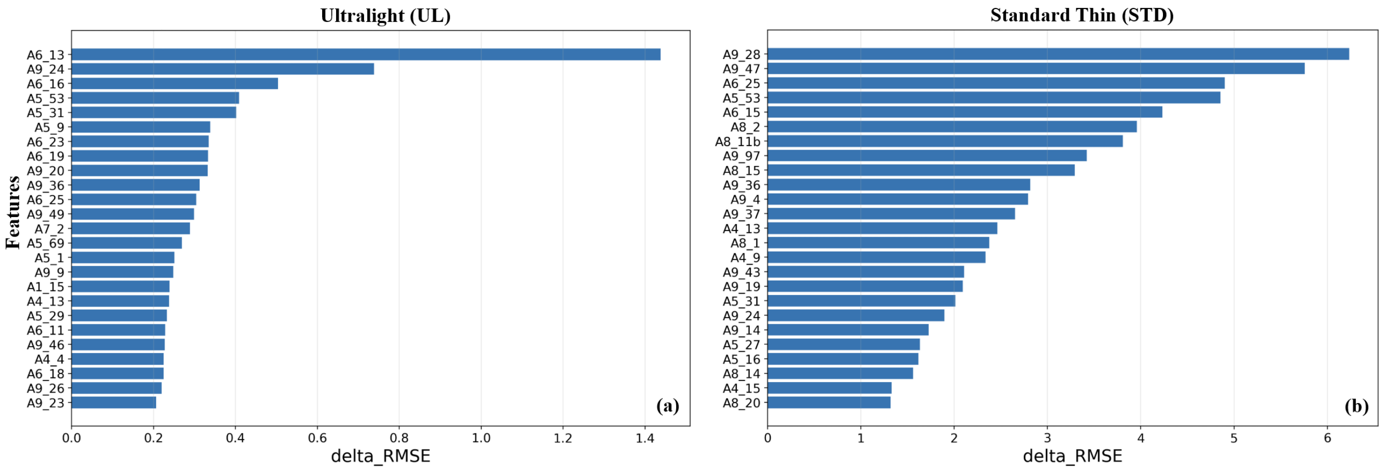

Figure 6. Global feature-importance rankings for Internal Bond prediction obtained from the strongest individual GBM evaluated during the AutoML search. (**a**) Ultralight MDF and (**b**) Standard Thin MDF. The rankings describe predictive relevance within the GBM and are presented as an auxiliary interpretation rather than as a direct explanation of every selected final model.

At the process level, the ranking pattern is consistent with the view that board quality develops through coupled interactions among moisture conditioning, resin application, and thermal-mechanical consolidation [7,24]. However, the reported importance values describe predictive relevance and should not be interpreted as causal effects.

A model-agnostic importance analysis applied directly to each selected model would be needed to determine whether the same ranking structure is retained across the complete predictive pipeline.

To assess whether this structure was retained in the final selected model, permutation feature importance (PFI) and SHAP values were calculated directly from the ensemble prediction function on the independent test set. For IB, the ensemble-level permutation analysis ranked A9_24, A5_1, A6_55 and A6_13 as the main predictors, with test-set RMSE increases of 1.489 ± 0.674, 1.424 ± 0.444, 1.349 ± 0.458 and 0.819 ± 0.343, respectively. The model-agnostic SHAP analysis identified the same four variables as the dominant contributors. Ranking concordance across the training, validation and test partitions was moderate, with Kendall's $W = 0.609$. Despite variability among predictors with small importance, the four dominant variables remained within the first four positions in every partition.

For VSC, A9_66 was consistently the leading predictor, followed by A6_29 and A5_57. Permuting A9_66 increased test RMSE by 0.168 ± 0.017, equivalent to 11.57% of the baseline test RMSE. The PFI and SHAP rankings were strongly correlated for VSC, with Spearman's $\rho = 0.765$, and eight variables were shared by their respective top-10 sets. Ranking stability across data partitions was high, with Kendall's W = 0.861 and pairwise Spearman correlations ranging from 0.744 to 0.843.

3.6. Inspection-Oriented Interpretation

The results show that industrial DCS data contain information that is useful for estimating IB and VSC before laboratory confirmation. Within the scope of the available data, the models are most appropriately viewed as continuous process-monitoring tools rather than as conformity classifiers.

For IB, the principal operational pattern was systematic over-quality. The central values of both product distributions exceeded their respective upper operating reference limits, with the largest deviation observed for Standard Thin panels. This result identifies a potential opportunity to reduce quality giveaway by adjusting resin dosage, thermal input, pressing conditions, or related operating variables while preserving the required IB level. Any such adjustment would require controlled industrial validation before implementation.

The current dataset does not support a reliable assessment of sensitivity, specificity, precision, false-negative rate, or inspection cost because near-threshold and non-conforming observations were poorly represented. Consequently, the models cannot yet be used to justify a reduction in destructive testing or to replace formal conformity assessment.

Their supported role is to provide an additional indication of process behavior, identify persistent departures from the desired quality range, and assist the review of operating periods associated with excessive or unstable quality. A prospective study containing sufficient observations near and below the acceptance thresholds is required to validate conformity detection, sampling-reduction strategies, and inspection-cost trade-offs.

4. Discussion

The results demonstrate that industrial DCS data can support inspection-oriented predictive quality modeling in continuous MDF manufacturing when the production line is treated as an integrated system of coupled subsystems rather than a collection of independent unit operations. The differential predictability of VSC and IB, the product-class-specific error structure, and the physical coherence of the feature-importance rankings collectively reflect the distributed nature of quality formation across the nine production stages analyzed in this study.

4.1. VSC Predictability and Its Physical Basis

Vertical Density Profile Index was predicted with lower error than Internal Bond across both product families, a result that is consistent with the physical mechanisms governing each response. VSC is closely linked to drying stability, resin and additive dosing, steam conditions, and thermal operating regimes process stages that are comparatively well instrumented in the studied DCS architecture. The most relevant predictors for VSC included variables from the dryer discharge moisture control (`A6_29`), dryer differential pressure, steam pressure at the dryer inlet, and resin-line flow rates. These variables directly reflect the moisture removal and thermal history that govern density development through the panel thickness during drying and pressing. VSC is therefore tractable from routine sensor signals [7,24].

The close match between validation and test errors for the VSC-UL model (RMSE: 1.41 vs. 1.39; MAE: 1.08 vs. 1.11) indicates stable generalization, suggesting that the underlying process–quality relationship is sufficiently captured by the available DCS signals and that the temporal variability of those signals across the training period represents the range encountered at test time.

4.2. IB Predictability and Emergent Mechanical Behavior

Internal Bond was harder to predict than VSC, especially for STD panels. IB is an emergent mechanical response that depends on fiber morphology, resin distribution, adhesive curing kinetics, heat and mass transfer during pressing, and vertical density profile development [14,36]. Several of these mechanisms are only indirectly observable through routine DCS tags: standard process historians do not record core-layer temperature evolution, fiber-level resin coverage, or cross-thickness density gradients. The model must therefore infer bonding quality from indirect proxies rather than from direct measurements of the mechanisms that determine IB.

This interpretive gap is more pronounced in STD panels, where reduced thickness increases sensitivity to localized disturbances in mat formation, moisture redistribution, and press closure dynamics. The larger errors for STD RMSE of 78.93 kPa versus 27.41 kPa for UL are consistent with findings in the broader MDF literature showing that thin boards have limited tolerance to local variations in mat distribution and compression history, and that small deviations in these stages produce disproportionately large changes in bonding performance [7,37].

The stronger IB performance for UL panels suggests that the available process tags provide a more stable representation of the mechanisms governing bonding behavior in that product family. The higher bulk-to-thickness ratio in UL panels reduces the relative influence of surface-layer and core-layer density gradients on measured IB, making the response less sensitive to localized press dynamics not captured by the historian. This structural argument is supported by the observation that the most relevant IB predictors for UL were concentrated in thermal conditioning, resin transport, and press cooling, which are more uniformly sensed along the continuous press than core-specific curing behavior.

4.3. Feature Importance and the Systems-Oriented Interpretation

The global importance rankings are physically coherent across both product families and both quality targets. For UL panels, the most influential tags included variables associated with dust-to-process flow (`A6_13`), press cooling temperature (`A9_24`), dryer differential pressure (`A6_14`–`A6_16`), defibrator chamber pressure (`A5_52`–`A5_53`), blow-valve behavior (`A5_31`), ECOR resin-line flow (`A5_2`), dryer-inlet steam pressure (`A6_23`–`A6_24`), and press steam conditions (`A9_57`). These variables link predictive performance to furnish flow stability, moisture removal, fiber transport, resin delivery, and thermal conditioning before final consolidation.

For STD panels, the highest-ranked variables were concentrated in hot-press heating circuits (`A9_26`–`A9_43`), compression circuits (`A9_45`–`A9_49`), dryer pressure behavior, defibrator pressure, mat humidification (`A8_1`–`A8_2`), and forming-head position (`A8_8`–`A8_9`). The prominence of heating-circuit temperature, compression-circuit response, press steam pressure, and forming-head outlet position is consistent with the greater sensitivity of thin boards to interactions between mat preparation and press thermodynamics, as identified in process-level studies of continuous flat-pressing systems [7,26].

These rankings are consistent with findings from large-scale data-driven analyses of MDF manufacturing, in which flash-tube dryer, mat forming, and hot-pressing variables were identified as the primary contributors to density and IB outcomes across thousands of production records [37]. The convergence of results across methodologies ensemble ML on DCS data in this study versus regularized regression on a much larger historian in the cited work reinforces the physical credibility of the importance structure reported here.

The importance rankings should nonetheless be interpreted as indicators of global predictive relevance within the fitted models, not as evidence of direct causality. Variables that appear highly ranked may reflect correlated operating regimes or shared control loops rather than independent physical mechanisms. The value of the rankings lies in directing process-engineering attention to the stages of the line that carry the most quality-relevant information under current instrumentation, not in establishing mechanistic pathways.

From a systems perspective, the recurrence of variables from drying, chemical defibration, forming, and pressing across both product families supports the core argument of this study: final MDF quality is not determined by any single control variable but by the combined effect of interconnected process subsystems distributed along the production line [7,8]. Moisture conditioning in A6–A7 affects resin cure kinetics and heat transfer in A9; resin and additive dosing in A5 influences bond formation during pressing; mat forming in A8 controls uniformity and basis weight, which determine compression response; pressing in A9 integrates all upstream variability into the final density and curing state. The stacked ensemble captures this distributed structure through nonlinear combinations of signals from multiple subsystems, which is precisely why ensemble methods outperformed single-stage models in all four prediction tasks.

4.4. Operational Interpretation and Inspection Role

From an industrial standpoint, the reported error levels indicate that the models are more suitable for inspection-oriented decision support than for replacing laboratory testing, consistent with the design intent stated in Section 2.8 [10,38]. Their operational value lies in reducing the delay between process drift and quality verification. For VSC, the relatively stable prediction errors across both product families suggest that the model can support near-real-time pre-screening as part of a broader quality-assurance workflow. For IB, the model should be applied with greater caution: UL panels can be screened with moderate confidence, while STD panels should be treated primarily as a risk-stratification context, flagging production intervals that warrant priority laboratory verification.

Deviations in variables related to dryer pressure, steam conditions, resin-line flow, forming-head position, humidification, press temperature, and compression response should be treated as process states with elevated relevance for quality monitoring. This operational logic connects the predictive model to the inspection planning cycle: when these variables signal atypical states, the probability of quality drift is higher, and targeted laboratory testing is likely to be more informative than uniform sampling [39,40].

The percentage-error stratification by quality band (Table 8) supports this interpretation. The balanced error distribution across low-, normal-, and over-quality regimes in UL panels indicates that the model does not systematically fail in any single quality region, which is a prerequisite for inspection use. A model that is accurate only in the normal-quality regime would provide no useful signal at the boundaries where intervention is most needed. The maximum error of 17.26% for IB-UL and 5.14% for VSC-UL defines the practical uncertainty envelope within which inspection decisions must be made.

Table 8. Performance summary for Ultralight MDF panels, including dataset sizes, validation and test errors, and percentage errors by quality band.

Metric	Training	Validation	Testing
IB—Ultralight			
Observations	1189	329	162
Predictor variables	55	55	55
RMSE (kPa)	–	41.24	27.41
MAE (kPa)	–	35.59	18.71
Mean error, low quality (%)	–	–	3.16
Mean error, normal quality (%)	–	–	2.98
Mean error, high quality (%)	–	–	2.82
Maximum error (%)	–	–	17.26
VSC—Ultralight			
Observations	1195	327	158
Predictor variables	72	72	72
RMSE (index)	–	1.41	1.39
MAE (index)	–	1.08	1.11
Mean error, low quality (%)	–	–	1.31
Mean error, normal quality (%)	–	–	1.29
Mean error, high quality (%)	–	–	1.26
Maximum error (%)	–	–	5.14

4.5. Limitations and Directions for Future Work

Several limitations of the current framework should be acknowledged. First, the data originate from routine industrial operation, where laboratory measurements are sparse relative to DCS signal frequency. The imbalance between predictor density and response density constrains model complexity and limits the detection of short-term quality transients. Second, several physical mechanisms central to IB formation core-layer bonding, fiber-level resin distribution, and vertical density profile development are only indirectly represented by standard DCS instrumentation [14,36]. Third, stacked and ensemble-based models improve predictive performance but reduce direct mechanistic interpretability; the importance rankings provide directional guidance but do not quantify causal contributions.

Future work should address these limitations along three complementary directions. The first is richer process representation: incorporating inline measurements of mat moisture distribution, press-gap evolution, core-layer temperature, and density profile would provide more direct observability of the mechanisms that govern IB, particularly in thin boards. The second is temporal modeling: explicit residence-time alignment, process-lag estimation, and sequential modeling of the material trajectory through the production line could improve temporal consistency and reduce prediction error for responses that integrate upstream variability over extended time windows [24,31]. The third is physics-informed modeling: hybrid approaches that embed heat transfer, moisture migration, resin curing, or press consolidation knowledge directly into the model architecture could improve both accuracy and interpretability, particularly for IB prediction in thin MDF products where purely data-driven methods face fundamental observability limits [41].

5. Conclusions

This study developed and evaluated an inspection-oriented predictive quality framework for continuous MDF manufacturing using industrial Distributed Control System (DCS) data and automated machine learning. The framework was designed to operate as a decision-support component within a broader quality-assurance system, linking process sensing, model-based interpretation, and inspection planning across a nine-stage production line treated as an integrated, coupled system.

The following conclusions are drawn from the experimental results:

1. **DCS data support useful quality estimates when the pipeline is carefully designed.** Process historian variables can provide reliable early estimates of selected quality attributes provided that preprocessing, collinearity control, target-specific feature selection, and product-family separation are applied systematically. The proposed pipeline RF-based imputation, Pearson collinearity filtering at $|r| \geq 0.8$, importance-based pruning, and H2O AutoML with stacked ensembles is transferable to other continuous wood-based panel lines with comparable DCS architectures.
2. **VSC is a robust target for near-real-time predictive monitoring.** Vertical Density Profile Index was the most consistently predicted quality variable across both Ultra-light (UL) and Standard Thin (STD) panels, with test RMSE of 1.39 and 1.78 (index units) respectively, and balanced percentage errors across quality bands. Its close connection to drying stability, steam pressure, thermal conditions, and resin dosing makes it directly traceable from routine sensor signals and a suitable candidate for operational deployment.
3. **IB prediction is feasible for UL panels but remains a risk-screening tool for STD panels.** Internal Bond was harder to predict, particularly for Standard Thin panels (test RMSE: 78.93 kPa vs. 27.41 kPa for UL), confirming that bonding strength is governed by mechanisms that are only indirectly observable through standard DCS instrumentation: fiber morphology, resin distribution, mat uniformity, moisture-dependent heat transfer, curing progression, and vertical density profile development [14,36]. For UL panels, the IB model provides sufficient accuracy for pre-screening. For STD panels, the model is best used to flag production intervals warranting priority laboratory verification rather than as a direct quality estimator.
4. **Feature importance rankings are physically coherent and process-stage-specific.** The most influential predictors for UL were concentrated in drying behavior, press cooling temperature, dryer pressure balance, resin-line flow, defibrator pressure, blow-valve behavior, and steam conditions. For STD panels, the dominant predictors shifted toward press heating circuits, compression circuits, dryer differential pressure, mat humidification, and forming-head position. These patterns are consistent with large-scale data-driven analyses of MDF manufacturing [37], and confirm that predictive performance arises from the interaction of multiple process stages rather than from any single sensor signal.
5. **A systems perspective is necessary and sufficient for framing MDF quality prediction.** Final board quality is not determined by isolated control variables but by the coupled effect of interconnected subsystems spanning fiber preparation, chemical application, drying, forming, and hot pressing [7,8]. Treating the production line as an integrated system rather than a collection of independent unit operations is a methodological prerequisite. It also explains why the importance rankings and error patterns differ between product families in the way they do.
6. **The models function best as an inspection-support layer, not as a compliance substitute.** Operationally, the framework identifies production intervals with elevated quality risk, prioritizes destructive sampling, and reduces the delay between process drift and laboratory confirmation [10,38]. Formal laboratory testing remains the basis for compliance decisions; the predictive layer improves the responsiveness and targeting of that testing without replacing it.

Future work should address three limitations identified in this study. First, richer process representation including inline measurements of mat moisture distribution, press-gap evolution, core-layer temperature, and vertical density profile would improve IB prediction in thin panels by providing direct observability of the mechanisms currently inferred from indirect proxies. Second, explicit temporal modeling through residence-time alignment and process-lag estimation would improve prediction consistency across production regimes and reduce sensitivity to batch-timestamp approximations [31]. Third, physics-informed hybrid modeling approaches that embed heat-transfer, resin-curing, or press-consolidation knowledge into the learning architecture could improve both accuracy and interpretability for responses that depend on mechanisms not directly sensed by routine DCS instrumentation [41].

Collectively, these advances would support broader deployment of predictive quality frameworks in continuous wood-based panel manufacturing as components of Industry 4.0 cyber-physical production systems, where process sensing, model-based interpretation, and inspection planning are integrated into a unified, adaptive quality-assurance architecture [8,40].

Author Contributions: Conceptualization, R.A.-G. and F.R.-L.; Methodology, R.A.-G., F.R.-L. and J.Z.B.; Software, R.A.-G., F.R.-L. and M.A.C.V.-C.; Validation, R.A.-G., F.R.-L. and S.E.R.-M.; Formal analysis, R.A.-G. and F.R.-L.; Investigation, R.A.-G., F.R.-L. and G.R.E.; Data curation, R.A.-G., F.R.-L. and M.A.C.V.-C.; Visualization, R.A.-G. and F.R.-L.; Writing—original draft preparation, R.A.-G. and F.R.-L.; Writing—review and editing, R.A.-G., F.R.-L. and S.E.R.-M.; Supervision, F.R.-L. and G.R.E. All authors have read and agreed to the published version of the manuscript.

Funding: F.R.-L. and R.A.-G. acknowledge the support of the Agencia Nacional de Investigación y Desarrollo (ANID), Chile, through FONDEQUIP grant number EQM220137, which provided the high-performance computing infrastructure used in this study, and of the Universidad del Bío-Bío.

Institutional Review Board Statement: No applicable.

Informed Consent Statement: No applicable.

Data Availability Statement: The dataset supporting the findings of this study is deposited in Zenodo and can be cited as [42]. The dataset contains industrial manufacturing data from medium-density fiberboard (MDF) production, including process variables, internal bond strength (IB), VSC measurements, and additional process attribute variables used for predictive modeling and quality analysis. Due to confidentiality and industrial data-sharing restrictions, the dataset is not publicly accessible but may be made available upon reasonable request through the access procedure described in the Zenodo repository.

Acknowledgments: During the preparation of this work the authors used ChatGPT (GPT-5.6 Sol, OpenAI, San Francisco, CA, USA) and Claude (Anthropic, San Francisco, CA, USA) in order to improve language and readability, and to assist with the preparation of the figure plotting code. After using these tools, the authors reviewed and edited the content as needed and take full responsibility for the content of the publication.

Conflicts of Interest: Author Javier Zarate Bertoglio was employed by Empresa Packing Bio Bio. The remaining authors declare that the research was conducted in the absence of any commercial or financial relationships that could be construed as a potential conflict of interest.

Abbreviations

The following abbreviations are used in this manuscript:

AI	Artificial Intelligence
ANN	Artificial Neural Network
AutoML	Automated Machine Learning
CARB	California Air Resources Board
DCS	Distributed Control System
GBM	Gradient Boosting Machine
GLM	Generalized Linear Model

IB	Internal Bond strength
MAE	Mean Absolute Error
MDF	Medium-Density Fiberboard
ML	Machine Learning
MOE	Modulus of Elasticity
MOR	Modulus of Rupture
PLC	Programmable Logic Controller
PQ	Predictive Quality
RF	Random Forest
RMSE	Root Mean Squared Error
STD	Standard Thin MDF panels
UL	Ultralight MDF panels
UF	Urea–Formaldehyde resin
VSC	Vertical Density Profile Index

Appendix A

Appendix A provides the dictionary of process variables used in this study. The variables correspond to DCS tags collected from equipment and sensors distributed across the MDF production line, covering the main operational stages: wood preparation, fiber preparation, defibration, chemical application, drying, forming, and hot pressing. For each process tag, the dictionary reports the original plant identifier, a descriptive label, and the coded variable name used during preprocessing, feature selection, and model development. This structure ensures traceability between the industrial historian records and the machine-learning predictors, while also supporting process-level interpretation of the models. The recorded variables describe key operating conditions such as flow rates, pressures, temperatures, humidity, resin and additive dosing, mat properties, press settings, and compression-related signals, which together represent the observable state of the continuous MDF manufacturing system.

Table A1. Dictionary of process tags and variables used in the study.

Tag	Description	Variable
E_677FI6726_PV	Effluent inlet flow	A1_1
E_ES0201_PV	Dry chip reclaimer levelling roll load control	A1_2
E_ES0221_PV	Levelling roll load control	A1_3
E_M0201M01EI_PV	Fresh chip reclaimer screw current	A1_4
E_M0201M01RPM_PV	Fresh chip reclaimer screw speed	A1_5
E_M0201M02EI_PV	Fresh chip reclaimer slewing current	A1_6
E_M0201M02SI_PV	Fresh chip reclaimer slewing speed	A1_7
E_M0202M09RPM_PV	Dry chip reclaimer metering screw speed	A1_8
E_RSIC0200_PV	Fresh chip reclaimer speed control	A1_9
E_RSIC0230_PV	Dry chip metering screw speed control	A1_10
E_SIC0233_PV	Sawdust silo discharge No. 1 speed control	A1_11
E_WI0206_PV	Fresh chip flow indication	A1_12
E_WI0207_PV	Dry chip flow indication	A1_13
H_EI_52_21_PV	General 220 kV line power (breaker 52-21)	A1_14
H_PIA0280_PV	Industrial water network pressure	A1_15
H_PIA0281_PV	Air network pressure	A1_16
P_EI_SUBESTAC2_BAT_PV	MDF2 substation No. 2 battery bank voltage	A1_17
E_LC0202_PV	Chip wash circulation tank level control	A2_1
E_LIA0232_PV	Sawdust silo level indication and alarm	A2_2
E_LIC0225_PV	Sawdust (PRS) metering bin level control	A2_3

Table A1. *Cont.*

Tag	Description	Variable
E_LIC0232_PV	Sawdust silo level indication	A2_4
E_M0237M010203RPM_PV	Sawdust metering bin screws No. 1, No. 2 and No. 3 speed	A2_5
E_M0237M010203SI_PV	Sawdust metering bin screws No. 1, No. 2 and No. 3 speed	A2_6
E_M0238M01RPM_PV	Sawdust weigh-scale conveyor speed	A2_7
E_M0250M02RPM_PV	Sawdust silo outfeed screw No. 1 speed	A2_8
E_M0250M02SI_PV	Sawdust silo outfeed screw No. 1 speed	A2_9
E_M0250M03RPM_PV	Sawdust silo outfeed screw No. 2 speed	A2_10
E_M0250M03SI_PV	Sawdust silo outfeed screw No. 2 speed	A2_11
E_M0257_IIC_01_PV	Robox current	A2_12
E_PIA0242_PV	Sawdust blower line No. 1 pressure	A2_13
E_PIA0243_PV	Sawdust blower line No. 2 pressure	A2_14
E_RWIC0226_PV	Sawdust flow control	A2_15
E_SICM0221_03_PV	Sawdust silo A screw speed control	A2_16
E_SICM0221_04_PV	Sawdust silo B screw speed control	A2_17
E_SICM0237_01_02_PV	Sawdust metering bin screws No. 1 and No. 2 speed control	A2_18
E_SICM0238_01_PV	Sawdust weigh conveyor speed control	A2_19
P_AIC003_PV	Clean water tank pH	A2_20
P_FIC008_PV	Clean water pump flow	A2_21
H_FIC0336_PV	Mixing screw steam flow	A3_1
H_LICA0300_PV	Steaming bin level control	A3_2
H_LICA0304_PV	Sawdust metering bin level control	A3_3
H_M0301M01SI_PV	Steaming bin discharge screw No. 1 speed	A3_4
H_M0301M03SI_PV	Steaming bin discharge screw No. 3 speed	A3_5
H_M0301M05SI_PV	Steaming bin discharge screw No. 5 speed	A3_6
H_M0302M01SI_PV	Sawdust metering bin screw No. 1 speed	A3_7
H_M0302M03SI_PV	Sawdust metering bin screw No. 3 speed	A3_8
H_M0303M01SI_PV	Mixing screw conveyor speed	A3_9
H_WI0385_PV	Sawdust flow (t/h)	A3_10
H_EI0322_PV	Plug feed screw current	A4_1
H_EI0324_PV	Preheater discharge screw current	A4_2
H_FI0310_PV	Preheater steam flow	A4_3
H_FI0326_PV	Total 6 bar steam flow	A4_4
H_FI0380_PV	Total 12.5 bar steam flow	A4_5
H_GHIC0308_PV	Preheater hoist position and RTC	A4_6
H_LC0342_PV	Drain tank level	A4_7
H_LICA0303_PV	ADI inlet chute level control	A4_8
H_LICA0307_PV	Preheater level control	A4_9
H_PIC0309_PV	Preheater steam pressure	A4_10
H_SI0321_PV	Plug feed screw speed	A4_11
H_TI0332_PV	Preheater average temperature	A4_12
H_TI0333_PV	Plug feed screw flush water temperature	A4_13
H_WI0335_PV	Preheater discharge screw flow 324	A4_14
PI_306_PV	PI_306 cone valve pressure	A4_15
H_WI0335_PV2	Preheater discharge screw flow 335	A4_14b
H_DPIC0311_PV	Defibrator differential pressure	A5_1
H_ECOR_GLINEFLOWSUM_PV	ECOR resin lines actual flow sum	A5_2
H_ECOR_L1_FLOW_PV	ECOR line 1 flow variable	A5_3
H_ECOR_L1_POS_PV	ECOR line 1 position variable	A5_4
H_ECOR_L10_FLOW_PV	ECOR line 10 flow variable	A5_5
H_ECOR_L10_POS_PV	ECOR line 10 position variable	A5_6
H_ECOR_L2_FLOW_PV	ECOR line 2 flow variable	A5_7
H_ECOR_L2_POS_PV	ECOR line 2 position variable	A5_8
H_ECOR_L3_FLOW_PV	ECOR line 3 flow variable	A5_9
H_ECOR_L3_POS_PV	ECOR line 3 position variable	A5_10
H_ECOR_L4_FLOW_PV	ECOR line 4 flow variable	A5_11

Table A1. *Cont.*

Tag	Description	Variable
H_ECOR_L4_POS_PV	ECOR line 4 position variable	A5_12
H_ECOR_L5_FLOW_PV	ECOR line 5 flow variable	A5_13
H_ECOR_L5_POS_PV	ECOR line 5 position variable	A5_14
H_ECOR_L6_FLOW_PV	ECOR line 6 flow variable	A5_15
H_ECOR_L6_POS_PV	ECOR line 6 position variable	A5_16
H_ECOR_L7_FLOW_PV	ECOR line 7 flow variable	A5_17
H_ECOR_L7_POS_PV	ECOR line 7 position variable	A5_18
H_ECOR_L8_FLOW_PV	ECOR line 8 flow variable	A5_19
H_ECOR_L8_POS_PV	ECOR line 8 position variable	A5_20
H_ECOR_L9_FLOW_PV	ECOR line 9 flow variable	A5_21
H_ECOR_L9_POS_PV	ECOR line 9 position variable	A5_22
H_ECOR_STEAMPRESSURE_PV	ECOR steam pressure	A5_23
H_EI0325_PV	Defibrator feeder current	A5_24
H_EIC0368_PV	Main motor power and SEC	A5_25
H_FI0312_PV	Defibrator steam flow	A5_26
H_FI0487_PV	ECOR steam flow	A5_27
H_FIA0328_PV	Defibrator mechanical seal steam flow	A5_28
H_GI0346_PV	Defibrator rotor position	A5_29
H_GIA0360_PV	Defibrator touchpoint vibration detector	A5_30
H_HIC0314_PV	Blow valve	A5_31
H_LIA_0483_PV	Resin tank 2 level indication	A5_32
H_LIA_0485_PV	Resin tank 3 level indication	A5_33
H_LIA0440_PV	Emulsion tank No. 1 level	A5_34
H_LIA0441_PV	Emulsion tank No. 2 level	A5_35
H_LIA0481_PV	Raw resin tank 1 level	A5_36
H_LIA0483_PV	Raw resin tank 2 level	A5_37
H_LIA0485_PV	Raw resin tank 3 level	A5_38
H_LIC0412_PV	Prepared resin level	A5_39
H_LICA0449_PV	Prepared scavenger level	A5_40
H_M0402M01SI_PV	Resin transfer pump No. 1 speed	A5_41
H_M0402M02SI_PV	Resin transfer pump No. 2 speed	A5_42
H_M0402M05SI_PV	Resin dosing pump No. 1 speed	A5_43
H_M0402M06SI_PV	Resin dosing pump No. 2 speed	A5_44
H_M0402M10SI_PV	Fungicide metering pump speed	A5_45
H_M0403M03SI_PV	Hardener metering pump speed	A5_46
H_M0404M03SI_PV	Scavenger metering pump speed	A5_47
H_M0407M01SI_PV	Melted wax metering pump No. 1 speed	A5_48
H_M0407M02SI_PV	Melted wax metering pump No. 2 speed	A5_49
H_M0408M01SI_PV	Emulsion pump No. 1 speed	A5_50
H_M0408M03SI_PV	Emulsion pump No. 3 speed	A5_51
H_PI0345_B_PV	Defibrator B chamber pressure	A5_52
H_PI0345_PV	Defibrator A chamber pressure	A5_53
H_PIA0486_PV	Ecoresinator line pressure	A5_54
H_PIC0421_PV	Wax steam pressure	A5_55
H_R_390_PV	Steam t/h to fiber t/h ratio	A5_56
H_RFIC0401_1_PV	Melted wax pump No. 1 flow	A5_57
H_RFIC0401_2_PV	Melted wax pump No. 2 flow	A5_58
H_RFIC0404_PV	Raw resin flow No. 1	A5_59
H_RFIC0405_PV	Raw resin flow No. 2	A5_60
H_RFIC0408_PV	Prepared resin flow	A5_61
H_RFIC0409_PV	Scavenger flow	A5_62
H_RFIC0414_PV	Dilution water flow	A5_63
H_RFICA0407_PV	Hardener flow	A5_64
H_RFICA0433_PV	Emulsion flow	A5_65
H_TIC0466_PV	Wax feeding line No. 1 temperature	A5_66

Table A1. *Cont.*

Tag	Description	Variable
H_TIC0467_PV	Wax feeding line No. 2 temperature	A5_67
H_TIC0468_PV	Wax return line temperature	A5_68
H_XIA0344_PV	Defibrator vibration detector	A5_69
O_EIC0368_PV	Main motor power and SEC (filtered)	A5_70
E_PIA0224_PV	15 bar steam pressure from boiler	A6_2
E_PIA0250_PV	36 bar steam pressure from boiler, process value	A6_3
E_PIA0252_PV	4.5 bar steam pressure from boiler	A6_4
H_DPI_504_PV	Boiler silo dust filter differential pressure	A6_5
H_FI_15BAR_PV	15 bar steam flow from boiler	A6_6
H_FI_4BAR_PV	4.5 bar steam flow from boiler	A6_7
H_LICA0107_PV	Condensate return level control	A6_8
H_LICA0107B_PV	Condensate return level control	A6_9
H_TIA0225_PV	14 bar steam line temperature	A6_10
H_TIA0251_PV	36 bar steam temperature from boiler	A6_11
H_TIA0253_PV	4.5 bar steam temperature from boiler	A6_12
H_WI0386_PV	Dust-to-process flow (t/h)	A6_13
J_DPIA_501A_PV	Dryer zone 1–2 differential pressure	A6_14
J_DPIA_501B_PV	Dryer zone 3–4 differential pressure	A6_15
J_DPIA_501C_PV	Dryer zone 5–6 differential pressure	A6_16
J_FICA0501_PV	Dryer inlet airflow control	A6_17
I0705_PV	Fiber conditioning transport air inlet humidity	A6_18
J_MI0705B_PV	Fiber conditioning transport air inlet temperature	A6_19
J_PI0550_PV	Press flash steam tank pressure 50	A6_20
J_PI0551_PV	Press flash steam tank pressure 51	A6_21
J_PI0552_PV	Press flash steam tank pressure 52	A6_22
J_PIA0526_PV	4.5 bar steam pressure at dryer inlet	A6_23
J_PIA0527_PV	15 bar steam pressure at dryer inlet	A6_24
J_PIA0550_PV	Press steam tank pressure	A6_25
J_PIA0551_PV	Flash steam tank pressure	A6_26
J_PIC0514_PV	Dryer LP steam pressure	A6_27
J_PIC0518_PV	Dryer HP steam pressure	A6_28
J_RMIC0505_PV	Dryer discharge moisture indication and control	A6_29
J_RTICA0502_PV	Dryer inlet air temperature control	A6_30
J_RTICA0502_TE01_PV	Dryer inlet air temperature control	A6_31
J_RTICA0502_TE02_PV	Dryer inlet air temperature control	A6_32
J_RTICA0502_TE03_PV	Dryer inlet air temperature control	A6_33
J_RTICA0502_TE04_PV	Dryer inlet air temperature control	A6_34
J_RTICA0503_PV	Dryer outlet air temperature control	A6_35
J_RTICA0503_TE01_PV	Dryer outlet air temperature control	A6_36
J_RTICA0503_TE02_PV	Dryer outlet air temperature control	A6_37
J_SIC0509_PV	Dryer discharge conveyor speed control	A6_38
J_TIA0524_01_PV	4.5 bar steam temperature at dryer inlet	A6_39
J_TIA0524_02_PV	4.5 bar steam temperature at dryer outlet	A6_40
J_TIA0525_01_PV	15 bar steam temperature at dryer inlet	A6_41
J_TIA0525_02_PV	15 bar steam temperature at dryer outlet	A6_42
J_TIC0703_PV	Fiber conditioning system heat exchanger outlet temperature	A6_43
J_TICA0520_PV	Dryer discharge conveyor temperature No. 1	A6_44
J_TICA0520_TE02_PV	Dryer discharge conveyor temperature No. 2	A6_45
J_TICA0520_TE03_PV	Dryer discharge conveyor temperature No. 3	A6_46
J_TICA0520_TE04_PV	Dryer discharge conveyor temperature No. 4	A6_47
J_TICA0520_TE05_PV	Dryer discharge conveyor temperature No. 5	A6_48
J_TICA0520_TE06_PV	Dryer discharge conveyor temperature No. 6	A6_49
J_TICA0520_TE07_PV	Dryer discharge conveyor temperature No. 7	A6_50
J_TICA0520_TE08_PV	Dryer discharge conveyor temperature No. 8	A6_51
J_TICA0520_TE09_PV	Dryer discharge conveyor temperature No. 9	A6_52

Table A1. *Cont.*

Tag	Description	Variable
J_TICA0520_TE10_PV	Dryer discharge conveyor temperature No. 10	A6_53
J_TICA0520_TE11_PV	Dryer discharge conveyor temperature No. 11	A6_54
J_XIA0517_PV	Dryer fan vibration indication	A6_55
D_WI031_TACTUAL_PV	31E1 dust weight to process	A6_1b
J_FIC0702_PV	Z-sifter recirculation airflow control	A7_1
J_PICA0701_PV	Z-sifter air pressure control	A7_2
J_FIC0737A_PV	FIC_0737A lower IMAL humidifier flow	A8_1
J_FIC0837A_PV	FIC_0837A upper IMAL humidifier flow	A8_2
J_LIC0530_PV	Mat former level	A8_3
L_BOARD_TEMP_PV	Mat temperature	A8_4
L_DIA0804_PV	Mat density gauge indication	A8_5
L_GIC0722_GE02_PV	Forming head inlet position, right	A8_6
L_GIC0722_PV	Forming head inlet position, left	A8_7
L_GIC0723_GT01_PV	Forming head outlet position, right	A8_8
L_GIC0723_GT02_PV	Forming head outlet position control	A8_9
L_GIC0723_GT02_PV2	Forming head outlet position control	A8_10
L_M0801M01SI_PV	Precompressor upper drive	A8_12
L_M0823M01SI_PV	Press infeed conveyor	A8_13
L_MIC0730_PV	Forming conveyor moisture indication and control	A8_14
L_SIC0712_PV	Dosing bin bottom belt conveyor speed control	A8_15
L_SIC0726_PV	Forming conveyor speed control	A8_16
L_TI0835_PV	Fiber mat temperature	A8_17
L_WIC0728_PV	Forming conveyor mat weigh-scale weight control	A8_18
O_FORMING_MAT_DENSITY_PV	Forming mat density	A8_19
O_FORMING_MAT_HEIGHT_PV	Forming mat height (measured)	A8_20
O_FORMING_MAT_WEIGHT_PV	Forming mat weight	A8_21
L_LIA0710_PV2	Dosing bin level indication	A8_11b
L_MIC0730_PV	Forming conveyor moisture indication and control	A8_14c
L_WIC0728_PV	Forming conveyor mat weigh-scale weight control	A8_18c
ACTADDWIDTHADJ	Width adjustment	A9_1
ACTDRVCURRENTMAINDRVBOT	Main drive bottom current	A9_2
ACTDRVCURRENTMAINDRVTOP	Main drive top current	A9_3
ACTDRVPOWERMAINDRVBOT	Main drive bottom power consumption	A9_4
ACTDRVPOWERMAINDRVTOP	Main drive top power consumption	A9_5
ACTDRVSPEEDBOT	Bottom speed	A9_6
ACTDRVSPEEDTOP	Top speed	A9_7
ACTFBCTRLROLLCENTERBOTINMM	Center control roll bottom position (mm)	A9_8
ACTFBCTRLROLLCENTERTOPINMM	Center control roll top position (mm)	A9_9
ACTFBCTRLROLLINFEEDBOTINMM	Infeed control roll bottom position (mm)	A9_10
ACTFBCTRLROLLINFEEDTOPINMM	Infeed control roll top position (mm)	A9_11
ACTFBDRUMPOSINFEEDBOTINMM	Infeed drum bottom position (mm)	A9_12
ACTFBDRUMPOSINFEEDTOPINMM	Infeed drum top position (mm)	A9_13
ACTFBDRUMPOSOUTFEEDBOTLEFT	Outfeed drum bottom-left position	A9_14
ACTFBDRUMPOSOUTFEEDBOTRIGHT	Outfeed drum bottom-right position	A9_15
ACTFBDRUMPOSOUTFEEDTOPLEFT	Outfeed drum top-left position	A9_16
ACTFBDRUMPOSOUTFEEDTOPRIGHT	Outfeed drum top-right position	A9_17
ACTFBINFEEDADJLEFT	Infeed adjustment, left side (upper drum height)	A9_18
ACTFBINFEEDADJRIGHT	Infeed adjustment, right side (upper drum height)	A9_19
ACTFBTRACKINGPRESSUREBOTLEFTBAR	Bottom-left tracking pressure (bar)	A9_20
ACTFBTRACKINGPRESSUREBOTRIGHTBAR	Bottom-right tracking pressure (bar)	A9_21
ACTFBTRACKINGPRESSURETOPLEFTBAR	Top-left tracking pressure (bar)	A9_22
ACTFBTRACKINGPRESSURETOPRIGHTBAR	Top-right tracking pressure (bar)	A9_23
ACTHTTEMPCOOLINGAREAINFEED	Cooling area inlet temperature	A9_24
ACTHTTEMPCOOLINGAREAOUTFEED	Cooling area outlet temperature	A9_25
ACTHTTEMPHEATINGCIRCUIT1BOT	Heating circuit 1 bottom temperature	A9_26

Table A1. *Cont.*

Tag	Description	Variable
ACTHTTEMPHEATINGCIRCUIT1FEED	Heating circuit 1 feeding-pipe temperature	A9_27
ACTHTTEMPHEATINGCIRCUIT1TOP	Heating circuit 1 top temperature	A9_28
ACTHTTEMPHEATINGCIRCUIT2BOT	Heating circuit 2 bottom temperature	A9_29
ACTHTTEMPHEATINGCIRCUIT2FEED	Heating circuit 2 feeding-pipe temperature	A9_30
ACTHTTEMPHEATINGCIRCUIT2TOP	Heating circuit 2 top temperature	A9_31
ACTHTTEMPHEATINGCIRCUIT3BOT	Heating circuit 3 bottom temperature	A9_32
ACTHTTEMPHEATINGCIRCUIT3FEED	Heating circuit 3 feeding-pipe temperature	A9_33
ACTHTTEMPHEATINGCIRCUIT3TOP	Heating circuit 3 top temperature	A9_34
ACTHTTEMPHEATINGCIRCUIT4BOT	Heating circuit 4 bottom temperature	A9_35
ACTHTTEMPHEATINGCIRCUIT4FEED	Heating circuit 4 feeding-pipe temperature	A9_36
ACTHTTEMPHEATINGCIRCUIT4TOP	Heating circuit 4 top temperature	A9_37
ACTHTTEMPHEATINGCIRCUIT5BOT	Heating circuit 5 bottom temperature	A9_38
ACTHTTEMPHEATINGCIRCUIT5FEED	Heating circuit 5 feeding-pipe temperature	A9_39
ACTHTTEMPHEATINGCIRCUIT5TOP	Heating circuit 5 top temperature	A9_40
ACTHTTEMPHEATINGCIRCUIT6BOT	Heating circuit 6 bottom temperature	A9_41
ACTHTTEMPHEATINGCIRCUIT6FEED	Heating circuit 6 feeding-pipe temperature	A9_42
ACTHTTEMPHEATINGCIRCUIT6TOP	Heating circuit 6 top temperature	A9_43
ACTHTTEMPPRESSUREPOTCOOL	Pressure pot cooling temperature	A9_44
ACTPRDCOMPRESSIONCIRCUIT01	Actual compression circuit 1	A9_45
ACTPRDCOMPRESSIONCIRCUIT02	Actual compression circuit 2	A9_46
ACTPRDCOMPRESSIONCIRCUIT03	Actual compression circuit 3	A9_47
ACTPRDCOMPRESSIONCIRCUIT04	Actual compression circuit 4	A9_48
ACTPRDCOMPRESSIONCIRCUIT05	Actual compression circuit 5	A9_49
ACTPRDEDGEOILPRESSUREC1	Actual edge oil pressure, circuit No. 1	A9_50
ACTPRDEDGEOILPRESSUREC2	Actual edge oil pressure, circuit No. 2	A9_51
ACTPRDEDGEOILPRESSUREC3	Actual edge oil pressure, circuit No. 3	A9_52
ACTPRDEDGEOILPRESSUREC4	Actual edge oil pressure, circuit No. 4	A9_53
ACTPRDHUMIDITY	Humidity	A9_54
ACTPRDWEIGHT	Product weight	A9_55
ACTSTEAMFLOW	Actual 36 bar steam flow	A9_56
ACTSTEAMPRESSURE	Actual 36 bar steam pressure	A9_57
ACTSTEAMTEMPERATURE	Actual 36 bar steam temperature	A9_58
CALAUTO_ENCODER_01R	CALAUTO encoder 01R	A9_59
CALAUTO_ENCODER_03R	CALAUTO encoder 03R	A9_60
CALAUTO_ENCODER_05R	CALAUTO encoder 05R	A9_61
CALAUTO_ENCODER_07R	CALAUTO encoder 07R	A9_62
CALAUTO_ENCODER_09R	CALAUTO encoder 09R	A9_63
CALAUTO_ENCODER_11R	CALAUTO encoder 11R	A9_64
CALAUTO_ENCODER_13R	CALAUTO encoder 13R	A9_65
CALAUTO_ENCODER_15R	CALAUTO encoder 15R	A9_66
CALAUTO_ENCODER_17R	CALAUTO encoder 17R	A9_67
CALAUTO_ENCODER_19R	CALAUTO encoder 19R	A9_68
CALAUTO_ENCODER_20L	CALAUTO encoder 20L	A9_69
CALAUTO_ENCODER_21R	CALAUTO encoder 21R	A9_70
CALAUTO_ENCODER_22L	CALAUTO encoder 22L	A9_71
CALAUTO_ENCODER_23R	CALAUTO encoder 23R	A9_72
CALAUTO_ENCODER_24L	CALAUTO encoder 24L	A9_73
CALAUTO_ENCODER_25R	CALAUTO encoder 25R	A9_74
CALAUTO_ENCODER_26L	CALAUTO encoder 26L	A9_75
CALAUTO_ENCODER_27R	CALAUTO encoder 27R	A9_76
CALAUTO_ENCODER_28L	CALAUTO encoder 28L	A9_77
CALAUTO_ENCODER_29R	CALAUTO encoder 29R	A9_78
CALAUTO_ENCODER_30L	CALAUTO encoder 30L	A9_79
CALAUTO_ENCODER_31R	CALAUTO encoder 31R	A9_80
CALAUTO_ENCODER_32L	CALAUTO encoder 32L	A9_81

https://doi.org/10.3390/systems14080972

Table A1. *Cont.*

Tag	Description	Variable
CALAUTO_ENCODER_33L	CALAUTO encoder 33L	A9_82
CALAUTO_ENCODER_33R	CALAUTO encoder 33R	A9_83
CALAUTO_ENCODER_35L	CALAUTO encoder 35L	A9_84
CALAUTO_ENCODER_37L	CALAUTO encoder 37L	A9_85
CALAUTO_ENCODER_37R	CALAUTO encoder 37R	A9_86
CALAUTO_ENCODER_40L	CALAUTO encoder 40L	A9_87
CALAUTO_ENCODER_40R	CALAUTO encoder 40R	A9_88
CALAUTO_ENCODER_41L	CALAUTO encoder 41L	A9_89
CALAUTO_ENCODER_41R	CALAUTO encoder 41R	A9_90
CALAUTO_ENCODER_43L	CALAUTO encoder 43L	A9_91
CALAUTO_ENCODER_43R	CALAUTO encoder 43R	A9_92
CALAUTO_ENCODER_45L	CALAUTO encoder 45L	A9_93
CALAUTO_ENCODER_45R	CALAUTO encoder 45R	A9_94
CALAUTO_ENCODER_47L	CALAUTO encoder 47L	A9_95
CALAUTO_ENCODER_47R	CALAUTO encoder 47R	A9_96
H_FI_36BAR_PV	36 bar steam flow from boiler	A9_97
S9902A_PV	Press speed	A9_98
S9902A_PV1	Press speed analog output	A9_99
SETDRVSPEED	Forming belt speed setpoint	A9_100
SETHTTEMPCOOLINGAREA	Cooling area temperature setpoint	A9_101
SETHTTEMPHEATINGCIRCUIT1	Heating circuit 1 temperature setpoint	A9_102
SETHTTEMPHEATINGCIRCUIT2	Heating circuit 2 temperature setpoint	A9_103
SETHTTEMPHEATINGCIRCUIT3	Heating circuit 3 temperature setpoint	A9_104
SETHTTEMPHEATINGCIRCUIT4	Heating circuit 4 temperature setpoint	A9_105
SETHTTEMPHEATINGCIRCUIT5	Heating circuit 5 temperature setpoint	A9_106
SETHTTEMPHEATINGCIRCUIT6	Heating circuit 6 temperature setpoint	A9_107
SETHTTEMPHEATINGCIRCUIT7	Heating circuit 7 temperature setpoint	A9_108
SETHTTEMPPRESSUREPOTCOOL	Pressure pot cooling temperature setpoint	A9_109
SETPRDCOMPRESSIONCIRCUIT01	Compression circuit 1 setpoint	A9_110
SETPRDCOMPRESSIONCIRCUIT02	Compression circuit 2 setpoint	A9_111
SETPRDCOMPRESSIONCIRCUIT03	Compression circuit 3 setpoint	A9_112
SETPRDCOMPRESSIONCIRCUIT04	Compression circuit 4 setpoint	A9_113
SETPRDCOMPRESSIONCIRCUIT05	Compression circuit 5 setpoint	A9_114

References

1. Zeng, Q.; Lu, Q. ; Zhou, Y.; Chen, N.; Rao, J.; Fan, M. Circular development of recycled natural fibers from medium density fiberboard wastes. *J. Clean. Prod.* **2018**, *202*, 456–464. [CrossRef]
2. Garcia, R.; Calvez, I.; Koubaa, A.; Landry, V.; Cloutier, A. Sustainability, Circularity, and Innovation in Wood-based Panel Manufacturing in the 2020s. *Curr. For. Rep.* **2024**, *10*, 420–441. [CrossRef] [PubMed]
3. Çamlıbel, O.; Aydın, M.; Koç, E. Influences of oak utilization on the medium density fiberboard properties. *Maderas Cienc. Tecnol.* **2024**, *26*, 21. [CrossRef]
4. Benthien, J.; Heldner, S.; Ohlmeyer, M. Investigation of the interrelations between defibration conditions, fiber size and medium-density fiberboard (MDF) properties. *Eur. J. Wood Wood Prod.* **2017**, *75*, 215–232. [CrossRef]
5. Savov, V.; Antov, P.; Panchev, C.; Lubis, M.; Taghiyari, H. The Impact of Hydrolysis Regime on the Physical and Mechanical Characteristics of Medium-Density Fiberboards Manufactured from Recycled Wood Fibers. *Fibers* **2023**, *11*, 103. [CrossRef]
6. Rodríguez, G.E.; Bustos Ávila, C.; Cloutier, A. Physical and Mechanical Properties of Fiberboard Made of MDF Residues and Phase Change Materials. *Forests* **2024**, *15*, 802. [CrossRef]
7. Lv, Y.; Liu, Y.; Jing, W. Continuous Flat Pressing of MDF Quality Control Model Framework and Collaborative Programming Approach Based on Wood Fiber Hot Pressing Mechanism. *Front. Plant Sci.* **2022**, *13*, 851219. [CrossRef] [PubMed]
8. Oks, S.J.; Jalowski, M.; Lechner, M.; Mirschberger, S.; Merklein, M.; Vogel-Heuser, B.; Möslein, K.M. Cyber-physical systems in the context of industry 4.0: A review, categorization and outlook. *Inf. Syst. Front.* **2024**, *26*, 1731–1772. [CrossRef]
9. Wuest, T.; Weimer, D.; Irgens, C.; Thoben, K.D. Machine learning in manufacturing: Advantages, challenges, and applications. *Prod. Manuf. Res.* **2016**, *4*, 23–45. [CrossRef]

10. Tercan, H.; Meisen, T. Machine learning and deep learning based predictive quality in manufacturing: A systematic review. *J. Intell. Manuf.* **2022**, *33*, 1879–1905. [CrossRef]
11. Bertolini, M.; Mezzogori, D.; Neroni, M.; Zammori, F. Machine Learning for industrial applications: A comprehensive literature review. *Expert Syst. Appl.* **2021**, *175*, 114820. [CrossRef]
12. Md, A.Q.; Jha, K.; Haneef, S.; Sivaraman, A.K.; Tee, K.F. A Review on Data-Driven Quality Prediction in the Production Process with Machine Learning for Industry 4.0. *Processes* **2022**, *10*, 1966. [CrossRef]
13. Schmitt, J.; Bönig, J.; Borggräfe, T.; Beitinger, G.; Deuse, J. Predictive Model-Based Quality Inspection Using Machine Learning and Edge Cloud Computing. *Adv. Eng. Inform.* **2020**, *45*, 101101. [CrossRef]
14. André, N.; Cho, H.W.; Baek, S.H.; Jeong, M.K.; Young, T.M. Prediction of internal bond strength in a medium density fiberboard process using multivariate statistical methods and variable selection. *Wood Sci. Technol.* **2008**, *42*, 521–534. [CrossRef]
15. André, N.; Young, T.M. Real-Time Process Modeling of Particleboard Manufacture Using Variable Selection and Regression Methods Ensemble. *Eur. J. Wood Wood Prod.* **2013**, *71*, 361–370. [CrossRef]
16. Schubert, M.; Luković, M.; Christen, H. Prediction of Mechanical Properties of Wood Fiber Insulation Boards as a Function of Machine and Process Parameters by Random Forest. *Wood Sci. Technol.* **2020**, *54*, 703–713. [CrossRef]
17. Ismail, F.S. Neural Network-Based Prediction Models for Physical Properties of Oil Palm Medium Density Fiberboard. Ph.D. Thesis, Universiti Teknologi MARA, Shah Alam, Malaysia, 2015.
18. Nazerian, M.; Shirzaii, S.; Mohebbi Gargarii, R.; Vatankhah, E. Evaluation of mechanical and flame retardant properties of medium density fiberboard using artificial neural network. *CERNE* **2020**, *26*, 279–292. [CrossRef]
19. Phetkaew, T.; Watcharakan, T.; Hiziroglu, S.; Chaowana, P. Using Machine Learning as an Adaptive Controller Framework for Optimizing Properties of Particleboard. *Eur. J. Wood Wood Prod.* **2024**, *82*, 1061–1068. [CrossRef]
20. Krauß, J.; Pacheco, B.M.; Zang, H.M.; Schmitt, R.H. Automated Machine Learning for Predictive Quality in Production. *Procedia CIRP* **2020**, *93*, 443–448. [CrossRef]
21. Xu, Z.; Wang, Y.; Qiu, T.; Wang, X.; Zhu, N. The Vibration Dynamic Model for Blister Detection in Medium-Density Fiberboard. *Forests* **2024**, *15*, 1058. [CrossRef]
22. *EN 319*; Particleboards and Fibreboards. Determination of Tensile Strength Perpendicular to the Plane of the Board. European Committee for Standardization: Brussels, Belgium, 1993.
23. *ASTM D1037-12(2020)*; Standard Test Methods for Evaluating Properties of Wood-Base Fiber and Particle Panel Materials. ASTM International: West Conshohocken, PA, USA, 2020.
24. Boffadossi, R.; Leonesio, M.; Fagiano, L.; Bianchi, G. Prediction of power consumption from real process data of an industrial wood chip refining plant. *IFAC-PapersOnLine* **2023**, *56*, 8574–8579. [CrossRef]
25. Tuissi, L.; Ravasio, D.; Spinelli, S.; Ballarino, A. Neural Network Modeling of the Refining Motor Load for Medium-Density Fibreboard Production. In *Proceedings of the 2023 15th International Conference on Computer and Automation Engineering (ICCAE), Sydney, Australia, 3–5 March 2023*; IEEE: Piscataway, NJ, USA, 2023; pp. 519–523. [CrossRef]
26. Lv, Y.; Liu, Y.; Jing, W.; Woźniak, M.; Damaševičius, R.; Scherer, R.; Wei, W. Quality Control of the Continuous Hot Pressing Process of Medium Density Fiberboard Using Fuzzy Failure Mode and Effects Analysis. *Appl. Sci.* **2020**, *10*, 4627. [CrossRef]
27. Lv, Y.; Liu, Y.; Li, X.; Lu, L.; Malik, A. Automated Shape Correction for Wood Composites in Continuous Pressing. *Forests* **2024**, *15*, 1118. [CrossRef]
28. Szwajka, K.; Zielińska-Szwajka, J.; Trzepieciński, T. The Use of a Radial Basis Function Neural Network and Fuzzy Modelling in the Assessment of Surface Roughness in the MDF Milling Process. *Materials* **2023**, *16*, 5292. [CrossRef] [PubMed]
29. Demir, A.; Birinci, A.U.; Ozturk, H. Determination of the surface characteristics of medium density fibreboard processed with CNC machine and optimisation of CNC process parameters by using artificial neural network. *CIRP J. Manuf. Sci. Technol.* **2021**, *35*, 929–942. [CrossRef]
30. Gao, Y.; Hua, J.; Chen, G.; Cai, L.; Jia, N.; Zhu, L. Prediction of Fiber Quality Using Refining Parameters in Medium-density Fiberboard Production via the Support Vector Machine Algorithm. *BioResources* **2018**, *13*, 8184–8197. [CrossRef]
31. Cattaldo, M.; Ferrer, A.; Måge, I. Variable time delay estimation in continuous industrial processes. *Chemom. Intell. Lab. Syst.* **2024**, *246*, 105082. [CrossRef]
32. Munappy, A.; Bosch, J.; Olsson, H.H.; Arpteg, A.; Brinne, B. Data management for production quality deep learning models: Challenges and solutions. *J. Syst. Softw.* **2022**, *191*, 111359. [CrossRef]
33. Wang, T.; Zheng, R.; Li, M.; Cai, C.; Zhu, S.; Lou, Y. Deep learning based self-adaptive modeling of multimode continuous manufacturing processes and its application to rotary drying process. *J. Intell. Manuf.* **2024**, *36*, 3887–3922. [CrossRef]
34. Vela, D.; Sharp, A.; Zhang, R.; Nguyen, T.; Hoang, A.; Pianykh, O.S. Temporal quality degradation in AI models. *Sci. Rep.* **2022**, *12*, 11654. [CrossRef] [PubMed]
35. LeDell, E.; Gill, N. H2O AutoML: Scalable Automatic Machine Learning. Available online: https://www.automl.org/wp-content/uploads/2020/07/AutoML_2020_paper_61.pdf (accessed on 9 June 2026).

36. Gupta, A.; Jordan, P.J.; Pang, S. Modelling of the Development of the Vertical Density Profile of MDF during Hot Pressing. *Chem. Prod. Process Model.* **2007**, *2*, 2. [CrossRef]
37. Park, S.; Park, B.D.; Kim, Y. Big data analysis on manufacturing variables affecting properties of medium density fiberboard. *Eur. J. Wood Wood Prod.* **2024**, *82*, 483–492. [CrossRef]
38. Rydzi, S.; Zahradnikova, B.; Sutova, Z.; Ravas, M.; Hornacek, D.; Tanuska, P. A Predictive Quality Inspection Framework for the Manufacturing Process in the Context of Industry 4.0. *Sensors* **2024**, *24*, 5644. [CrossRef] [PubMed]
39. Soori, M.; Arezoo, B.; Dastres, R. AI-Based Decision Support Systems in Industry 4.0, a Review. *J. Econ. Technol.* **2024**, *1*, 73–90. [CrossRef]
40. Cassoli, B.; Schuh, G.; Lüttgens, D. Frameworks for Data-Driven Quality Management in Cyber-Physical Systems for Manufacturing: A Systematic Review. *Procedia CIRP* **2022**, *107*, 658–663. [CrossRef]
41. Farahani, M.A.; McCormick, M.R.; Gianinny, R.; Harik, R.; Wuest, T. Physics-Based and Data-Driven Hybrid Modeling in Manufacturing: A Review. *Prod. Manuf. Res.* **2024**, *12*, 2305358. [CrossRef]
42. Aedo, R. MDF Manufacturing Process Dataset for Machine Learning-Based Quality Optimization. 2026. Available online: https://zenodo.org/records/20611458 (accessed on 9 June 2026).